

Close Encounters of the Binary Kind: Signal Reconstruction Guarantees for Compressive Hadamard Sampling with Haar Wavelet Basis

A. Moshtaghpour* J. M. Bioucas-Dias† L. Jacques*

July 24, 2019

Abstract

We investigate the problems of 1-D and 2-D signal recovery from subsampled Hadamard measurements using Haar wavelet sparsity prior. These problems are of interest in, *e.g.*, computational imaging applications relying on optical multiplexing or single pixel imaging. However, the realization of such modalities is often hindered by the coherence between the Hadamard and Haar bases. The variable and multilevel density sampling strategies solve this issue by adjusting the subsampling process to the local and multilevel coherence, respectively, between the two bases; hence enabling successful signal recovery. In this work, we compute an explicit sample-complexity bound for Hadamard-Haar systems as well as uniform and non-uniform recovery guarantees; a seemingly missing result in the related literature. We explore the faithfulness of the numerical simulations to the theoretical results and show in a practically relevant instance, *e.g.*, single pixel camera, that the target signal can be obtained from a few Hadamard measurements.

Keywords: Hadamard transform, Haar wavelet, variable density sampling, compressive sensing.

1 Introduction

The theory of Compressed Sensing (CS), introduced by Donoho [1] and Candès and Tao [2], is now a versatile sampling paradigm in many real-world applications, *e.g.*, Magnetic Resonance Imaging (MRI) [3], fluorescence microscopy [4, 5], and imaging [6]. Mathematically, CS considers the problem of recovering a signal $\mathbf{x} \in \mathbb{C}^N$ from M noisy measurements

$$\mathbf{y} = \mathbf{A}\mathbf{x} + \mathbf{n} \in \mathbb{C}^M. \quad (1)$$

In (1), the matrix $\mathbf{A} \in \mathbb{C}^{M \times N}$ approximates the physical sensing process of \mathbf{x} , and \mathbf{n} denotes an additive noise vector. A typical goal in CS is minimizing the number of measurements M while guaranteeing the quality of the signal recovery. This is indeed a critical aspect of the applications of CS. For example, the number of measurements in MRI application can be translated into the X-ray dose, which has to be minimized.

*ISPGROUP, ICTEAM/ELEN, UCLouvain, Belgium (`{amirafshar.moshtaghpour, laurent.jacques}@uclouvain.be`). AM is funded by the FRIA/FNRS. LJ funded by the F.R.S.-FNRS.

In this paper, we tackle an important problem in the applications of CS theory: recovering a signal from subsampled Hadamard measurements using the Haar wavelet sparsity basis. In particular, in a wide range of imaging modalities, *e.g.*, optical multiplexing or single pixel camera [6], the sensing process can be modeled as taking measurements from the Hadamard transform. Moreover, considering the Haar wavelet basis paves the way to study other wavelet bases in combination with the Hadamard matrix. In this context, the main question becomes: how to design an optimum sampling strategy for subsampling the Hadamard measurements. Note that in this paper, the term “optimum” refers to a sampling strategy that minimizes the required number of measurements without degrading the quality of the signal reconstruction.

Traditional CS relying on orthonormal sensing systems [7] suggests selecting the rows of the sensing matrix (in our case, the Hadamard matrix) uniformly at random, *i.e.*, according to a Uniform Density Sampling (UDS). Unfortunately, this approach fails when the target signal is sparse or compressible in a basis, called sparsity basis, that is too coherent with the sensing basis (see Sec. 2). One example of this failure is the Hadamard-Haar system, where the sensing basis (Hadamard) is maximally coherent with the sparsity basis (Haar wavelet). This drawback is often called the “coherence barrier” in the literature [8].

Nevertheless, this barrier can be broken. Several empirical [9–11] and theoretical evidences [8, 12, 13] suggest using a non-uniform density sampling strategy [12–14], which densifies the subsampling of the lower Hadamard frequencies, to obtain superior signal reconstruction quality. In a general context, Krahmer and Ward [13] and Adcock *et al.* [12] arguably began to replace the notion of global coherence with its local versions, *i.e.*, *local coherence* and *multilevel coherence* parameters, respectively. The idea in these works is to discriminate the elements of the sensing basis (*e.g.*, Hadamard) in favor of those that are highly coherent with all the elements of the sparsity basis (*e.g.*, Haar).

Although there are other versions of non-uniform sampling strategies, *e.g.*, [14–17], we here focus on the framework of Krahmer and Ward [13], called here Variable Density Sampling (VDS), and the one of Adcock *et al.* [12], called here Multilevel Density Sampling (MDS). These allow us to derive suitable sampling strategies for Hadamard-Haar systems. Note that the term “VDS” is often used in the literature for other non-uniform density sampling strategies, while we here use VDS and MDS terms to distinguish the frameworks of [13] and [8, 12].

An important aspect of CS theory is the difference between *uniform* and *non-uniform*¹ (or fixed signal) recovery guarantees [18, Chapter 9]. The former is tightly connected to the Restricted Isometry Property (RIP) [19]. Essentially, a uniform recovery guarantee claims that a single draw of the sampling matrix is, with high probability, sufficient for the recovery of *all* sparse signals. A non-uniform recovery guarantee asserts that a single draw of the sampling matrix is, with high probability, sufficient for recovery of a *fixed* sparse signal.

This paper derives both uniform and non-uniform recovery guarantees for Hadamard-Haar systems and associated optimum sampling strategies. For uniform (and non-uniform) guarantee we resort to the VDS framework of Krahmer and Ward [13] (resp. MDS framework of Adcock *et al.* [12]).

¹A word of caution. Uniform and non-uniform density sampling strategies are related to the way the rows of a matrix are subsampled and should not be confused with uniform and non-uniform recovery guarantees.

1.1 Related Works

Non-uniform density sampling (theory and application): The idea of non-uniform density sampling dates back to the emergence of CS. Donoho in [1] proposed a two-level sampling approach for recovering wavelet coefficients, where the coarse wavelet scale coefficients are fully sampled while the remaining coefficients are subsampled with UDS strategy. This idea was later extended by Tsaig and Donoho in [20] to a multiscale setup. Puy *et al.* [14] advocated a convex optimization procedure for minimizing the coherence between the sensing and sparsity bases. A non-uniform density sampling approach is proposed by Wang and Arce in [21] based on the statistical models of natural images. Bigot *et al.* [15] introduced the notion of block sampling for CS, based on acquiring the blocks of measurements instead of isolated measurements; see also a similar study of Polak *et al.* [22]. Boyer *et al.* incorporated the idea of block sampling with structured sparsity in [16], whose stable and robust recovery guarantee was later proved by Adcock *et al.* in [23]. A RIP-based recovery guarantee is presented by Krahmer and Ward [13] based on the notion of *random bounded orthonormal systems* introduced in [18, 24]. The sampling strategy in [13] is controlled by the local coherence between the sensing and sparsity bases. Adcock *et al.* [12] provided a novel MDS scheme based on the local sparsity and multilevel coherence between the sensing and sparsity bases. A generalization of the RIP for MDS strategy of [12] in finite dimensions (and infinite dimensions) has been analyzed by Li and Adcock in [17] (resp. Adcock *et al.*, [25]).

Most of the works above also tackled the problem of signal recovery from subsampled Fourier measurements using wavelet sparsity basis (Fourier-Wavelet system), *e.g.*, [12–14, 16, 26]. In this context, the applications of non-uniform density sampling have shown promising results in MRI [3, 5, 27] and interferometric hyperspectral imaging [28–32].

Imaging applications of the Hadamard transform: The Hadamard matrix has become an emerging element in many computational imaging applications relying on optical multiplexing or single pixel imaging, such as Hadamard spectroscopy [4, 5, 33], lensless camera [34], 3-D video imaging [35], laser-based failure-analysis [36], compressive holography [37], single pixel Fourier transform interferometry [10, 11, 38], digital holography [39], intracranial electroencephalogram acquisition [9], single pixel camera [40], and micro-optoelectromechanical systems [41].

Most of the works above have already been designed based on different non-uniform sampling schemes, that can be categorized, based on the sampling designs, in four groups, *i.e.*, the rows of the Hadamard matrix are selected with respect to (i) UDS [33], (ii) MDS [5, 9, 10], (iii) low-pass sampling where the first M rows are selected [35, 39], and (iv) half-half sampling where the first $M/2$ rows are always selected and the other $M/2$ rows are selected uniformly at random among the rest of the rows [4]. Although all these works have obtained high quality signal recovery, they do not provide an explicit recovery guarantee.

Moreover, other contributions, *e.g.*, on video compressive sensing [42], 3-D imaging [43], remote sensing [44], terahertz imaging [45], and single pixel camera [6, 46], which utilize random binary patterns (*e.g.*, Bernoulli matrices) can potentially adopt Hadamard sensing with no hardware burden.

Hadamard-wavelet systems (theory): The recovery of 1-D signals that are sparse in an orthonormal wavelet basis (from subsampled Hadamard measurements) has been studied in [47] in the context of MDS. The problem of signal reconstruction from the Hadamard (or binary) measurements has recently received attention in other contexts than CS, *e.g.*, in generalized sampling

	Sensing basis			Sparsity basis				Signal dimension			Sampling strategy		Signal type		Recovery guarantee		Context	
	any orthonormal	Fourier	Hadamard	any orthonormal	Haar wavelet	Daubechies wavelet	orthogonal wavelet	1-D (vector)	2-D (matrix)	d-D (tensor)	VDS	MDS	finite-dimensional	infinite-dimensional	uniform	non-uniform	compressive sensing	generalized sampling
Krahmer and Ward [13]	✓	✓		✓	✓			✓	✓		✓		✓		✓		✓	
Adcock <i>et al.</i> [12]	✓	✓		✓			✓	✓				✓	✓			✓	✓	
Adcock <i>et al.</i> [26]		✓			✓			✓				✓	✓			✓	✓	
Li and Adcock [17]	✓	✓		✓	✓			✓				✓	✓		✓		✓	
Antun [47]			✓		✓	✓		✓				✓	✓		✓		✓	
Adcock <i>et al.</i> [25]	✓		✓	✓	✓		✓	✓				✓	✓		✓		✓	
Hansen and Thesing [54]			✓				✓		✓	—	—		✓		—	—		✓
Thesing and Hansen [55]			✓		✓				✓	—	—		✓		—	—		✓
Hansen and Terhaar [48]			✓				✓		✓	—	—		✓		—	—		✓
Thesing and Hansen [56]			✓			✓		✓			✓		✓				✓	
This work: Thm. 3			✓		✓			✓	✓		✓		✓		✓		✓	✓
This work: Thm. 4			✓		✓			✓	✓		✓		✓		✓		✓	✓

Table 1: Comparison between the state-of-the-art works and our contribution. In this table, we consider those contributions in the field of CS that are based on the local coherence (developed by Krahmer and Ward in [13]) and multilevel coherence (developed by Adcock *et al.* in [12]) parameters.

methods where the goal is to recover an infinite-dimensional signal from a full set of measurements (without subsampling) via a linear reconstruction. In this context, there exist several works where the sampling space is assumed to be the domain of Hadamard transform and the reconstruction takes place in the span of some wavelet basis (see, *e.g.*, [25, 48] and [49] for a survey). In this work, however, we address the recovery of both 1-D and 2-D finite-dimensional signals using the Haar wavelet sparsity basis. To the best of our knowledge, four other papers have addressed the relationship between the 1-D Hadamard and 1-D Haar wavelet bases [50–53]. In the next section, as well as Table 1, we compare our contribution with the state-of-the-art works.

1.2 Our Contributions

The main contributions of this paper are the followings:

- We provide uniform and non-uniform recovery guarantees for compressive Hadamard-Haar systems that are stable with respect to non-sparse signals and robust to the measurement noise. We build our analysis upon [13] (for the uniform guarantee) and upon [12] (for the non-uniform guarantee).
- The results cover the recovery of 1-D and 2-D signals. In the latter case, we treat two constructions of the 2-D Haar basis, *i.e.*, using the tensor product and multi-resolution analysis. We will prove that either construction results in a different optimum sampling strategy.
- By computing the exact values of the local and multilevel coherence parameters for Hadamard-Haar systems, we provide tight sample complexity bounds relatively to the VDS and MDS frameworks.

This work thus provides explicit CS strategies for Hadamard-Haar systems; an association that was seemingly not covered by the related literature (see, *e.g.*, Table 1). Our main results are presented in

Thm. 3 (for the uniform recovery guarantee) and in Thm. 4 (for the non-uniform guarantee). Note that this Hadamard-Haar sensing system has recently been applied to the CS of hyperspectral data with single pixel imaging (when the light illumination is spatially coded with Hadamard system) [10, 11], with improved recovery performances compared to UDS strategy. During the finalization of this paper, we became aware of this recent survey of Calderbank *et al.* [49] that pursue similar objectives. Compared to our result in Thm. 4, Thm. 5.8 in [49], which is stated from [56], covers the problem of infinite-dimensional signal recovery using Daubechies wavelets. Moreover, Fig. 3 in [49] advocates the same structure as in Fig. 5-right for infinite-dimensional 2-D Hadamard-Haar system. However, the mathematical expression in Prop. 2-(ii) for modeling those structures is original.

1.3 Paper Organization

This paper is organized as follows. We first provide a summary of the CS theory in Sec. 2, emphasizing on sensing strategies exploiting orthonormal bases (*e.g.*, Fourier or Hadamard), as well as the uniform and non-uniform signal recovery guarantees. In Sec. 3.2, after delivering a short introduction to the Hadamard and Haar wavelet bases, we present our main results in Thm. 3 and Thm. 4. Note that the technical proofs are postponed to Sec. 5. Finally, we conduct a series of numerical tests in Sec. 4, which confirms the efficiency of our analysis.

1.4 Notations

Domain dimensions are represented by capital letters, *e.g.*, K, M, N . Vectors and matrices are denoted by bold symbols. For a matrix $\mathbf{U} = [\mathbf{u}_1, \dots, \mathbf{u}_{N_2}] \in \mathbb{C}^{N_1 \times N_2}$, $\mathbf{u} = \text{vec}(\mathbf{U}) := [\mathbf{u}_1^\top, \dots, \mathbf{u}_{N_2}^\top]^\top \in \mathbb{C}^{N_1 N_2}$ corresponds to the folded vector representation of \mathbf{U} . When this is clear from the context, we assimilate a matrix in $\mathbb{C}^{N_1 \times N_2}$ with its vectorized version, *i.e.*, identifying \mathbf{U} with \mathbf{u} . For any matrix (or vector) $\mathbf{V} \in \mathbb{C}^{M \times N}$, \mathbf{V}^\top and \mathbf{V}^* represent the transposed and the conjugate transpose of \mathbf{V} , respectively, and $\mathbf{V} \otimes \mathbf{W}$ denotes the Kronecker product of two matrices \mathbf{V} and \mathbf{W} . The ℓ_p -norm of \mathbf{u} reads $\|\mathbf{u}\|_p := (\sum_i |u_i|^p)^{1/p}$, for $p \geq 1$, with $\|\mathbf{u}\| := \|\mathbf{u}\|_2$. For a matrix \mathbf{U} , $\|\mathbf{U}\|_{p,q} := \max_{\mathbf{x}} \{\|\mathbf{U}\mathbf{x}\|_q \text{ s.t. } \|\mathbf{x}\|_p = 1\}$, for $p, q \geq 1$. The identity matrix of dimension N is represented as \mathbf{I}_N . Similarly, $\mathbf{1}_N$ (or $\mathbf{0}_N$) describes a vector of length N with all components equal 1 (resp. 0); when the value of N is clear from the text we simply write $\mathbf{1}$ (resp. $\mathbf{0}$) for simplicity. By an abuse of convention, unless expressed differently, we consider that a set (or a subset) of indices is actually a *multiset*, *i.e.*, the repetition and ordering of the elements are allowed; the set cardinality thus considers the total number of (non-unique) multiset elements. For a subset $\Omega = \{\omega_j\}_{j=1}^M \subset \llbracket N \rrbracket := \{1, \dots, N\}$ of cardinality $|\Omega|$, the restriction operator is denoted by $\mathbf{P}_\Omega \in \{0, 1\}^{M \times N}$ with $(\mathbf{P}_\Omega \mathbf{x})_j = x_{\omega_j}$. Moreover, the mask operator is represented by $\bar{\mathbf{P}}_\Omega := \mathbf{P}_\Omega^\top \mathbf{P}_\Omega \in \{0, 1\}^{N \times N}$ with $(\bar{\mathbf{P}}_\Omega \mathbf{x})_j = x_j$ if $j \in \Omega$, and zero otherwise. The concatenation of two sets $\mathcal{S} = \{s_i\}_{i=1}^M$ and $\mathcal{T} = \{t_i\}_{i=1}^N$ is denoted by $\mathcal{S} \sqcup \mathcal{T} := \{s_1, \dots, s_M, t_1, \dots, t_N\}$. We thus have $\mathbf{P}_{\mathcal{S} \sqcup \mathcal{T}} \mathbf{u} = [\mathbf{P}_\mathcal{S}^\top, \mathbf{P}_\mathcal{T}^\top]^\top \mathbf{u}$. We define $\llbracket N \rrbracket_0 := \{0\} \sqcup \llbracket N \rrbracket$. The floor function $\lfloor u \rfloor$ outputs the greatest integer less than or equal to u . We use the asymptotic relations $f \lesssim g$ (or $f \gtrsim g$), if $f \leq cg$ (resp. $g \leq cf$) for two functions f and g and some value $c > 0$ independent of their parameters. In order to go back and forth between the 1-D and 2-D index representations $l \in \llbracket N_1 N_2 \rrbracket$ and $(l_1, l_2) \in \llbracket N_1 \rrbracket \times \llbracket N_2 \rrbracket$, respectively, we use the relation $l \xleftrightarrow{N_1, N_2} (l_1, l_2)$, meaning that $k = l_1 + N_1(l_2 - 1)$, $l_1 = (l - 1 \bmod N_1) + 1$, and $l_2 = \lfloor (l - 1)/N_1 \rfloor + 1$; when $N_1 = N_2 = N$ we simply write $l \xleftrightarrow{N} (l_1, l_2)$. The Cartesian product with *lexicographical* ordering of two sets $\mathcal{S}_1 \subset \llbracket N_1 \rrbracket$ and

$\mathcal{S}_2 \subset \llbracket N_2 \rrbracket$ is denoted by $\mathcal{S}_1 \times \mathcal{S}_2$. Moreover, $\overline{\mathcal{S}_1 \times \mathcal{S}_2} := \{i \in \llbracket N_1 N_2 \rrbracket : i \xleftrightarrow{N_1, N_2} (j, k), j \in \mathcal{S}_1, k \in \mathcal{S}_2\}$ converts the 2-tuple elements of $\mathcal{S}_1 \times \mathcal{S}_2$ to 1-tuple elements .

2 Compressed Sensing for Orthonormal Bases

We summarize here uniform and non-uniform recovery guarantees for CS of signals acquired from partial measurements in bounded orthonormal systems (*e.g.*, Fourier and Hadamard). We begin by recalling some limitations of the coherence-based analysis between two orthonormal systems, one used for the signal sensing and the other one for the sparse signal representation.

The need for non-uniform density sampling: Let $\mathbf{x} \in \mathbb{C}^N$ be a signal to be recovered from noisy compressive measurements

$$\mathbf{y} = \mathbf{P}_\Omega \Phi^* \mathbf{x} + \mathbf{n} \in \mathbb{C}^M, \quad (2)$$

where the sensing basis $\Phi \in \mathbb{C}^{N \times N}$ is an orthonormal basis (*e.g.*, Hadamard), $\Omega \subset \llbracket N \rrbracket$ is a set (or multiset) of indices chosen at random with $|\Omega| = M \ll N$, and \mathbf{n} is an additive observation noise.

In order to estimate \mathbf{x} from \mathbf{y} , CS theory requires three ingredients: (*i*) low-complexity prior information of the signal, (*ii*) efficient subsampling strategy of $\llbracket N \rrbracket$ for defining Ω , and (*iii*) a non-linear recovery algorithm which takes into account the low-complexity prior model. A typical low-complexity prior in real-world applications, *e.g.*, image processing and hyperspectral imaging, is that the target signal \mathbf{x} has a K -sparse or compressible (*i.e.*, well-approximated by a sparse signal) representation in a general orthonormal basis $\Psi \in \mathbb{C}^{N \times N}$ (*e.g.*, Haar wavelet), *i.e.*, $|\text{supp}(\Psi^* \mathbf{x})| \leq K$. In this context, by-now-traditional results in CS theory (*e.g.*, [18, Cor. 12.38] or [7]) state that in order to reconstruct K -sparse signals, one must draw

$$M \gtrsim N \mu^2(\Phi^* \Psi) K \log(N) \quad (3)$$

elements of Ω uniformly at random in $\llbracket N \rrbracket$, where

$$\mu(\mathbf{U}) := \max_{1 \leq i, j \leq N} |u_{i,j}| \in [1/\sqrt{N}, 1], \quad (4)$$

is the coherence of $\mathbf{U} \in \mathbb{C}^{N \times N}$. For coherent sensing and sparsity bases, *e.g.*, Hadamard and Haar wavelet bases, respectively, $\mu(\Phi^* \Psi) = 1$ and thus, $M \gtrsim N$ measurements are required for signal recovery, which prevents (at least in theory) any compression. This limitation is indeed related to the construction of Ω , *i.e.*, according to a Uniform Density Sampling (UDS).

As explained in Sec. 1.1, there exist fundamentally-different theoretical results that suggest a non-uniform density sampling in the case of coherent bases, with the same idea of breaking the coherence barrier (*e.g.*, [12–14, 16]). In this work we restrict our analysis to the VDS scheme of Krahmer and Ward [13] (for uniform guarantee) and the MDS scheme of Adcock *et al.* [12] (for non-uniform guarantee).

VDS and uniform recovery guarantee: Krahmer and Ward showed in [13] that the sample-complexity bound in (3) can be modified by assigning higher sampling probability to the columns

of the sensing basis Φ (or equivalently, to the rows of Φ^*) that are highly coherent with the columns of the sparsity basis Ψ . They have thus defined the *local coherence*

$$\mu_l^{\text{loc}} = \mu_l^{\text{loc}}(\Phi^* \Psi) := \max_{1 \leq j \leq N} |(\Phi^* \Psi)_{l,j}| \in [1/\sqrt{N}, 1], \quad \forall l \in \llbracket N \rrbracket, \quad (5)$$

with $\max_l \mu_l^{\text{loc}}(\Phi^* \Psi) = \mu(\Phi^* \Psi)$. In the sequel, we will denote the vector $\boldsymbol{\mu}^{\text{loc}} := [\mu_1^{\text{loc}}, \dots, \mu_N^{\text{loc}}]^\top$ formed by all local coherences. Krahmer and Ward [13] proved that this quantity determines a sufficient condition on the construction of the subsampling set Ω for most classes of recovery algorithms, *e.g.*, convex optimization [19], thresholding [57], and greedy [58] strategies. Therefore, we leverage Thm. 5.2 in [13] and combine it with Thm. 2.1 in [59] in order to provide the following self-contained recovery guarantee.

Theorem 1 (VDS and uniform recovery guarantee for CS, adapted from [13] and [59]). *Let $\Phi \in \mathbb{C}^{N \times N}$ and $\Psi \in \mathbb{C}^{N \times N}$ be orthonormal sensing and sparsity bases, respectively, with $\mu_l^{\text{loc}}(\Phi^* \Psi) \leq \kappa_l$ for some values $\kappa_l \in \mathbb{R}_+$. Let us define $\boldsymbol{\kappa} := [\kappa_1, \dots, \kappa_N]^\top$. Fix $\epsilon \in (0, 1]$ and $\delta < 1/\sqrt{2}$ and suppose $K \gtrsim \log(N)$,*

$$M \gtrsim \delta^{-2} \|\boldsymbol{\kappa}\|^2 K \log(\epsilon^{-1}), \quad (6)$$

and choose M (possibly not distinct) indices $l \in \Omega \subset \llbracket N \rrbracket$ *i.i.d.* with respect to the probability distribution η on $\llbracket N \rrbracket$ given by

$$\eta(l) := \frac{\kappa_l^2}{\|\boldsymbol{\kappa}\|^2}. \quad (7)$$

Consider the diagonal matrix $\mathbf{D} = \text{diag}(\mathbf{d}) \in \mathbb{R}^{M \times M}$ with $d_j = 1/\sqrt{\eta(\Omega_j)}$, $j \in \llbracket M \rrbracket$. With probability exceeding $1 - \epsilon$, for all $\mathbf{x} \in \mathbb{C}^N$ observed through the noisy CS model $\mathbf{y} = \mathbf{P}_\Omega \Phi^* \mathbf{x} + \mathbf{n}$ with $\|\mathbf{D}\mathbf{n}\| \leq \epsilon\sqrt{M}$, the solution $\hat{\mathbf{x}}$ of the program

$$\hat{\mathbf{x}} = \arg \min_{\mathbf{u} \in \mathbb{C}^N} \|\Psi^* \mathbf{u}\|_1 \text{ s. t. } \frac{1}{\sqrt{M}} \|\mathbf{D}(\mathbf{y} - \mathbf{P}_\Omega \Phi^* \mathbf{u})\| \leq \epsilon, \quad (8)$$

satisfies

$$\|\mathbf{x} - \hat{\mathbf{x}}\| \leq c_1 \frac{\sigma_K(\Psi^* \mathbf{x})_1}{\sqrt{K}} + c_2 \epsilon, \quad c_1 = 2^{\frac{\delta + \sqrt{\delta(1/\sqrt{2} - \delta)}}{1 - \sqrt{2}\delta}}, c_2 = \frac{2\sqrt{2(1+\delta)}}{1 - \sqrt{2}\delta},$$

where $\sigma_K(\mathbf{u})_1 := \|\mathbf{u} - \mathcal{H}_K(\mathbf{u})\|_1$ is the best K -term approximation error (in the ℓ_1 sense), and \mathcal{H}_K is the hard thresholding operator that maps all but the K largest-magnitude entries of the argument to zero. In particular, the reconstruction is exact, *i.e.*, $\hat{\mathbf{x}} = \mathbf{x}$, if \mathbf{x} is K -sparse and $\epsilon = 0$. Note that for $\delta = 1/3$, $c_1 < 2.58$, and $c_2 < 6.18$.

This recovery guarantee is uniform in the sense that a single construction of the measurement matrix $\mathbf{P}_\Omega \Phi^*$ with respect to the sample-complexity bound in (6) and sampling pmf in (7) is sufficient to ensure (with high probability) the recovery of all sparse vectors. This result is of interest in those applications of CS where sparsity (or compressibility) of the target signal is the only possible prior knowledge. In the following we describe a method, which takes into account local sparsity of the target signal.

MDS and non-uniform recovery guarantee Adcock and co-authors [12] have also advocated that the global notion of coherence in (4) and sparsity must be replaced by a proper local versions in order to obtain a better subsampling strategy.

To fix the ideas, we first introduce the CS setup proposed in [12]. For a fixed $r \in \mathbb{N}$ we decompose the signal (or sparsity) domain $\llbracket N \rrbracket$ into r disjoint *sparsity levels* $\mathcal{S} := \{\mathcal{S}_1, \dots, \mathcal{S}_r\}$ such that $\bigcup_{l=1}^r \mathcal{S}_l = \llbracket N \rrbracket$. Given a vector of sparsity parameters $\mathbf{k} = [k_1, \dots, k_r]^\top \in \mathbb{N}^r$, a vector $\mathbf{s} \in \mathbb{C}^N$ is called $(\mathcal{S}, \mathbf{k})$ -sparse-in-level, and we write $\mathbf{s} \in \Sigma_{\mathcal{S}, \mathbf{k}}$, if $|\text{supp } \mathbf{P}_{\mathcal{S}_l} \mathbf{s}| \leq k_l$ for all $l \in \llbracket r \rrbracket$. For an arbitrary vector \mathbf{s} , its $(\mathcal{S}, \mathbf{k})$ -approximation error is denoted by $\sigma_{\mathcal{S}, \mathbf{k}}(\mathbf{s}) := \min\{\|\mathbf{s} - \mathbf{z}\|_1 : \mathbf{z} \in \Sigma_{\mathcal{S}, \mathbf{k}}\} = \sum_l \sigma_{k_l}(\mathbf{P}_{\mathcal{S}_l} \mathbf{s})_1$. We quickly observe that the sparsity-in-level model reduces to the global sparsity model by setting $r = 1$ and $\mathcal{S} = \llbracket N \rrbracket$.

Similar to the sparsity domain, we decompose the sampling domain $\llbracket N \rrbracket$ into r disjoint *sampling levels* defined as $\mathcal{W} := \{\mathcal{W}_1, \dots, \mathcal{W}_r\}$ with $\bigcup_{l=1}^r \mathcal{W}_l = \llbracket N \rrbracket$. Given $\mathbf{m} = [m_1, \dots, m_r]^\top \in \mathbb{N}^r$, the set $\Omega_{\mathcal{W}, \mathbf{m}} := \bigcup_{t=1}^r \Omega_t$ provides an MDS scheme, or $(\mathcal{W}, \mathbf{m})$ -MDS, if, for each $1 \leq t \leq r$, $\Omega_t \subseteq \mathcal{W}_t$, $|\Omega_t| = m_t \leq |\mathcal{W}_t|$, and if the entries of Ω_t are chosen uniformly at random (without replacement) in \mathcal{W}_t .

We further need to define two quantities controlling the sample-complexity bound in MDS scheme (see below). Given an orthonormal matrix $\mathbf{U} \in \mathbb{C}^{N \times N}$ and local sparsity values \mathbf{k} , the t^{th} *relative sparsity* is defined as

$$K_t^{\mathcal{W}, \mathcal{S}}(\mathbf{U}, \mathbf{k}) = \max_{\mathbf{z} \in \Sigma_{\mathcal{S}, \mathbf{k}}: \|\mathbf{z}\|_\infty \leq 1} \|\mathbf{P}_{\mathcal{W}_t} \mathbf{U} \mathbf{z}\|^2. \quad (9)$$

In the cases where the computation of the exact relative sparsity values given in (9) is not feasible, one can instead upper bound it as stated in the next lemma, which is adapted from [26, Eq. 13].

Lemma 1. $\sqrt{K_t^{\mathcal{W}, \mathcal{S}}(\mathbf{U}, \mathbf{k})} \leq \sum_{l=1}^{|\mathcal{S}|} \|\mathbf{P}_{\mathcal{W}_t} \mathbf{U} \mathbf{P}_{\mathcal{S}_l}^\top\|_{2,2} \sqrt{k_l}$.

Moreover, the $(t, l)^{\text{th}}$ *multilevel coherence* of \mathbf{U} with respect to the sampling and sparsity levels \mathcal{W} and \mathcal{S} , respectively, is defined as

$$\mu_{t,l}^{\mathcal{W}, \mathcal{S}}(\mathbf{U}) := \mu(\mathbf{P}_{\mathcal{W}_t} \mathbf{U}) \mu(\mathbf{P}_{\mathcal{W}_t} \mathbf{U} \mathbf{P}_{\mathcal{S}_l}^\top). \quad (10)$$

Within this context, the following guarantee can be reformulated from [12, Thm. 4.4].

Theorem 2 (MDS and non-uniform recovery guarantee for CS, adapted from [12]). *Let $\Phi \in \mathbb{C}^{N \times N}$ and $\Psi \in \mathbb{C}^{N \times N}$ be orthonormal sensing and sparsity bases, respectively. Fix sampling and sparsity levels \mathcal{W} and \mathcal{S} , respectively. Let $\Omega = \Omega_{\mathcal{W}, \mathbf{m}}$ be a $(\mathcal{W}, \mathbf{m})$ -MDS and $(\mathcal{S}, \mathbf{k})$ be any pair such that the following holds: for $0 < \epsilon \leq \exp(-1)$, $K = \|\mathbf{k}\|_1$, \hat{m}_t is such that for all $l \in \llbracket \mathcal{S} \rrbracket$,*

$$1 \gtrsim \sum_{t=1}^r \left(\left(\frac{|\mathcal{W}_t|}{\hat{m}_t} - 1 \right) \mu_{t,l}^{\mathcal{W}, \mathcal{S}}(\Phi^* \Psi) K_t^{\mathcal{W}, \mathcal{S}}(\Phi^* \Psi, \mathbf{k}) \right), \quad (11)$$

and m_t such that for all $t \in \llbracket \mathcal{W} \rrbracket$,

$$m_t \gtrsim \hat{m}_t \log(K \epsilon^{-1}) \log(N), \quad (12)$$

$$m_t \gtrsim |\mathcal{W}_t| \left(\sum_{l=1}^r \mu_{t,l}^{\mathcal{W}, \mathcal{S}}(\Phi^* \Psi) k_l \right) \log(K \epsilon^{-1}) \log(N). \quad (13)$$

Given the noisy CS measurements $\mathbf{y} = \mathbf{P}_\Omega \Phi^* \mathbf{x} + \mathbf{n}$ with $\|\mathbf{n}\| \leq \epsilon$, suppose that $\hat{\mathbf{x}} \in \mathbb{C}^N$ is a minimizer of

$$\hat{\mathbf{x}} = \arg \min_{\mathbf{u} \in \mathbb{C}^N} \|\Psi^* \mathbf{u}\|_1 \text{ s.t. } \|\mathbf{y} - \mathbf{P}_\Omega \Phi^* \mathbf{u}\| \leq \epsilon. \quad (14)$$

Then, with probability exceeding $1 - \epsilon$, we have

$$\|\mathbf{x} - \hat{\mathbf{x}}\| \leq c_1 \sigma_{\mathcal{S}, \mathbf{k}}(\Psi^* \mathbf{x}) + c_2(1 + C\sqrt{K}) \varepsilon \sqrt{q}, \quad (15)$$

where $q := \max_t \frac{|W_t|}{m_t}$ for some constant $0 < c_1 \leq 22, 0 < c_2 \leq 11$, and where $0 \leq C \leq 3\sqrt{6} + \frac{4\sqrt{6}\sqrt{\log(6N\epsilon^{-1})}}{\log(N)}$.

We remark the main differences between this theorem and Thm. 1. First, Thm. 2 provides a non-uniform recovery guarantee: the measurement matrix $\mathbf{P}_\Omega \Phi^*$ satisfying the conditions of the proposition needs (in theory) to be redrawn when a new vector is to be recovered. Second, the MDS scheme requires a prior information about the local sparsity of the target signal; while the VDS scheme in Prop. 1 does not need such information. Third, the parameter ε in optimization program (14) is a bound on the observation noise power, while in the VDS scheme (8) it is a bound on the weighted noise power. However, we showed in [30, Thm. 2.5] that one can determine a bound on $\|\mathbf{D}\mathbf{n}\|$, which holds with controllable probability, and that depends on the $\|\mathbf{n}\|$, $\|\mathbf{n}\|_\infty$ (or on estimations bounding these quantities with high probability) and a parameter fixed by the pmf defining the VDS scheme.

3 The compressive sensing Hadamard-Haar problem

We now focus on a special case of the CS settings concerned by Thm. 1 and Thm. 2, where the sensing and sparsity bases are set as Hadamard and Haar wavelet bases, respectively. Before presenting the main results, we first recall the definitions of the 1-D, 2-D anisotropic, and 2-D isotropic Haar wavelet bases and Paley-ordered Hadamard matrix. These definitions are useful to develop the machinery of our contributions.

3.1 Haar and Hadamard Bases

1-D Discrete Haar Wavelet (DHW) basis: Fix $N = 2^r$ for some $r \in \mathbb{N}$. The DHW basis of \mathbb{R}^N consists of N vectors

$$\{\psi_j^{\text{1d}}\}_{j=1}^N := \{\bar{h}\} \cup \{h_{s,p}^{(1)} : 0 \leq s \leq r-1, 0 \leq p \leq 2^s - 1\} \subset \mathbb{R}^N,$$

where, for $\tau \in \llbracket N-1 \rrbracket_0$, $\bar{h}(\tau) := 2^{-r/2}$ is the constant (scaling) function and $h_{s,p}^{(1)}(\tau) := 2^{\frac{s-r}{2}} h(2^{s-r}\tau - p)$ is the wavelet function at scale (or resolution) s and position p , with $h(\tau)$ equals 1, -1, and 0 over $[0, 1/2)$, $[1/2, 1)$, and $\mathbb{R} \setminus [0, 1)$, respectively (see [60, Page 2], [61, Page 6], or [26]), *i.e.*,

$$h_{s,p}^{(1)}(\tau) = \begin{cases} 2^{\frac{s-r}{2}}, & \text{for } p2^{r-s} \leq \tau < (p + \frac{1}{2})2^{r-s}, \\ -2^{\frac{s-r}{2}}, & \text{for } (p + \frac{1}{2})2^{r-s} \leq \tau < (p+1)2^{r-s}, \\ 0, & \text{otherwise.} \end{cases} \quad (16)$$

In a matrix form, DHW basis in $\mathbb{R}^{N \times N}$ can be constructed [50, 51] from the recursive relation

$$\Psi_{\text{dhw}} := \mathbf{W}_r^{(1)} := \frac{1}{\sqrt{2}} \left[\mathbf{W}_{r-1}^{(1)} \otimes \begin{bmatrix} 1 \\ 1 \end{bmatrix}, \mathbf{I}_{2^{r-1}} \otimes \begin{bmatrix} 1 \\ -1 \end{bmatrix} \right], \quad \text{with } \mathbf{W}_0^{(1)} := [1], \quad (17)$$

which collects in its columns all the vectors of $\{\psi_j^{\text{1d}}\}_{j=1}^N$ (see Lemma 2).

In order to extend the DHW basis to the 2-D Haar wavelet basis, we need to define $N - 1$ window functions

$$h_{s,p}^{(0)}(\tau) = \begin{cases} 2^{\frac{s-r}{2}}, & \text{for } p2^{r-s} \leq \tau < (p+1)2^{r-s}, \\ 0, & \text{otherwise,} \end{cases} \quad (18)$$

for the resolution $0 \leq s \leq r-1$ and position $0 \leq p \leq 2^s - 1$ parameters. Similar to the construction of the DHW basis in (17), we define the matrix

$$\mathbf{W}_r^{(0)} := \frac{1}{\sqrt{2}} \left[\mathbf{W}_{r-1}^{(0)} \otimes \begin{bmatrix} 1 \\ 1 \end{bmatrix}, \mathbf{I}_{2^{r-1}} \otimes \begin{bmatrix} 1 \\ 1 \end{bmatrix} \right], \quad \text{with } \mathbf{W}_0^{(0)} := [1], \quad (19)$$

Which collects in its first column the vector \bar{h} and in the other columns all the vectors $\{h_{s,p}^{(0)}\}$ (see Lemma 2).

Associated with the DHW basis, the *1-D dyadic levels* $\mathcal{T}^{1d} := \{\mathcal{T}_l^{1d}\}_{l=0}^r$ gather coefficient indices with identical wavelet levels; they are defined as

$$\mathcal{T}_l^{1d} := \llbracket 2^l \rrbracket \setminus \llbracket 2^{l-1} \rrbracket, \quad \text{for } l \in \llbracket r \rrbracket, \quad \text{and } \mathcal{T}_0^{1d} := \{1\}, \quad (20)$$

with cardinality $|\mathcal{T}_l^{1d}| = 2^{l-1}$, for $l \in \llbracket r \rrbracket$. We also define left-complement of dyadic levels as $\mathcal{T}_{<l}^{1d} := \bigcup_{j=0}^{l-1} \mathcal{T}_j^{1d} = \llbracket 2^{l-1} \rrbracket$ for $l \in \llbracket r \rrbracket$ and $\mathcal{T}_{<0}^{1d} := \emptyset$. These levels are important to isolate the indices of the columns (components) of $\Psi_{\text{dhw}} = \mathbf{W}_r^{(1)}$ (resp. $(\Psi_{\text{dhw}})^\top \mathbf{x}$) associated with a given scale, as well as those of $\mathbf{W}_r^{(0)}$

Lemma 2. For $l \in \llbracket r \rrbracket_0$ and $a \in \{0, 1\}$, the matrix $\mathbf{W}_r^{(a)} \mathbf{P}_{\mathcal{T}_l^{1d}}^\top \in \mathbb{R}^{2^r \times |\mathcal{T}_l^{1d}|}$ collects in its columns all the vectors $\{h_{l-1,p}^{(a)}\}_{p=0}^{2^{l-1}-1}$, if $l \in \llbracket r \rrbracket$, and if $l = 0$, it collects \bar{h} in its single column.

Proof. See Sec. 5.1. □

There exist two natural ways to construct a 2-D wavelet basis from a 1-D basis, *i.e.*, by tensor product of two 1-D bases, and by following a multi-resolution analysis (see [60, Sec. 7.7], [62], or [63]), which amounts to multiplying all possible pairs of wavelet and scaling functions sharing the same resolution. We describe below those two approaches for 2-D Haar wavelet construction.

2-D Anisotropic Discrete Haar Wavelet (ADHW) basis: For the first approach, the tensor product of two DHW bases leads to an anisotropic 2-D DHW basis. For $N = 2^r$ and some $r \in \mathbb{N}$, we consider the scaling and wavelet functions \bar{h} and $h_{s,p}^{(1)}$ defined above, and we build the ADHW basis of \mathbb{R}^{N^2} as

$$\{\psi_j^{\text{aniso}}\}_{j=1}^{N^2} := \{\psi_{j_1}^{1d} \psi_{j_2}^{1d} : j \stackrel{N}{\iff} (j_1, j_2)\},$$

which provides N^2 possible functions. This basis is of interest for image compression [64], sparsity basis for MRI images [16], and sparsity basis for monochromatic images in fluorescence spectroscopy [30]. In particular, Neumann and von Sachs [65] showed that if a multi-dimensional signal has different degrees of smoothness in different directions, the tensor wavelet construction is a better choice for signal estimation.

In a matrix form, the ADHW basis in $\mathbb{R}^{N^2 \times N^2}$ can be constructed [60, 63] as

$$\Psi_{\text{adhw}} := \Psi_{\text{dhw}} \otimes \Psi_{\text{dhw}},$$

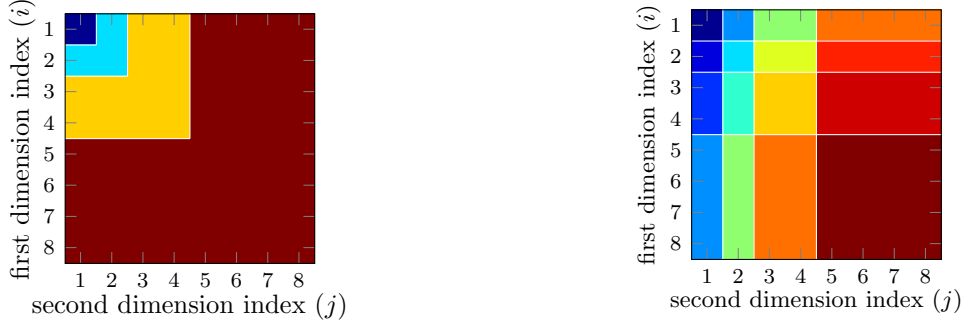


Figure 1: An example of the 2-D isotropic wavelet levels $\mathcal{T}_l^{\text{iso}}$ for $l \in \llbracket r \rrbracket_0$ (left) versus 2-D anisotropic wavelet levels $\mathcal{T}_l^{\text{aniso}}$ for $l \in \llbracket (r+1)^2 \rrbracket$ (right) with $N = 8$ (or $r = 3$). Each area represents the subset of pairs of indices (i, j) that belong to a level l .

where Ψ_{adhw} collects in its columns all the vectors of $\{\psi_j^{\text{aniso}}\}_{j=1}^{N^2}$. Associated with the ADHW basis, we define the 2-D anisotropic wavelet levels $\mathcal{T}^{\text{aniso}} := \{\mathcal{T}_l^{\text{aniso}}\}_{l=1}^{r^2}$ where $\mathcal{T}_l^{\text{aniso}} := \overline{\mathcal{T}_{l_1}^{\text{1d}} \times \mathcal{T}_{l_2}^{\text{1d}}}$, for $l \in \llbracket (r+1)^2 \rrbracket$ and $l_1, l_2 \in \llbracket r \rrbracket_0$, with the relation $l \xleftrightarrow{r+1} (l_1+1, l_2+1)$ and hence $|\mathcal{T}_l^{\text{aniso}}| = |\mathcal{T}_{l_1}^{\text{1d}}| \cdot |\mathcal{T}_{l_2}^{\text{1d}}|$. These levels thus gather the indices of wavelet coefficients associated with the constant resolution (see the illustration on Fig. 1-right for $N = 8$).

Remark 1. According to the construction of Ψ_{adhw} and $\mathcal{T}^{\text{aniso}}$, one can use Lemma 2 and Lemma 3 to show that

$$\Psi_{\text{adhw}} \mathbf{P}_{\mathcal{T}_l^{\text{aniso}}}^\top = \left(\Psi_{\text{dhw}} \mathbf{P}_{\mathcal{T}_{l_2}^{\text{1d}}}^\top \right) \otimes \left(\Psi_{\text{dhw}} \mathbf{P}_{\mathcal{T}_{l_1}^{\text{1d}}}^\top \right), \text{ for } l \xleftrightarrow{r+1} (l_1+1, l_2+1).$$

2-D Isotropic Discrete Haar Wavelet (IDHW) basis: The second type of the 2-D DHW basis is built from a multi-resolution analysis [60]. Fix $N = 2^r$ for some $r \in \mathbb{N}$. Let \bar{h} , $h^{(1)}$, and $h^{(0)}$ be the scaling, wavelet, and window functions defined above. Following [60] the IDHW basis $\{\psi_j^{\text{iso}}\}_{j=1}^{N^2}$ of \mathbb{R}^{N^2} consists of the functions

$$\{\phi^{(00)}\} \cup \{\phi_{s, (p_1, p_2)}^{(ab)} : 0 \leq s \leq r-1, 0 \leq p_1, p_2 \leq 2^s - 1, (a, b) \in \{0, 1\}^2 \setminus \{0, 0\}\},$$

such that

$$\phi^{(00)}(\tau_1, \tau_2) = \bar{h}(\tau_1) \bar{h}(\tau_2), \quad (21)$$

$$\phi_{s, (p_1, p_2)}^{(ab)}(\tau_1, \tau_2) = h_{s, p_1}^{(a)}(\tau_1) h_{s, p_2}^{(b)}(\tau_2), \quad (22)$$

where $0 \leq s \leq r-1$ and $0 \leq p_1, p_2 \leq 2^s - 1$ are the resolution and position indices, respectively, *i.e.*, there are N^2 possible functions.

To construct the orthonormal matrix $\Psi_{\text{idhw}} \in \mathbb{R}^{N^2 \times N^2}$ associated with the 2-D IDHW basis, we leverage the 1-D partitions $\mathcal{T}_l^{\text{1d}}$ defined above so that the column ordering of Ψ_{idhw} will ease any further column selection (*e.g.*, in Sec. 3.2).

We first define the submatrices

$$\Psi_l^{(ab)} := \left(\mathbf{W}^{(a)} \mathbf{P}_{\mathcal{T}_l^{\text{1d}}}^\top \right) \otimes \left(\mathbf{W}^{(b)} \mathbf{P}_{\mathcal{T}_l^{\text{1d}}}^\top \right) \in \mathbb{R}^{N^2 \times |\mathcal{T}_l^{\text{1d}}|^2}, \quad l \in \llbracket r \rrbracket, (a, b) \in \{0, 1\}^2 \setminus \{(0, 0)\}$$

and $\Psi_0^{(00)} := \mathbf{1}_{N^2}$. For each level l , these submatrices clearly contain all the functions $\{\phi_{l-1, (p_1, p_2)}^{(ab)} : p_1, p_2 \in \llbracket 2^l - 1 \rrbracket_0\}$. Moreover, since $\mathcal{T}_{<l}^{1d} = \llbracket 2^{l-1} \rrbracket$ and $\mathcal{T}_l^{1d} = \llbracket 2^l \rrbracket / \llbracket 2^{l-1} \rrbracket$, the following disjoint sets

$$\mathcal{T}_0^{(00)} := \overline{\mathcal{T}_0^{1d} \times \mathcal{T}_0^{1d}}, \quad \mathcal{T}_l^{(11)} := \overline{\mathcal{T}_l^{1d} \times \mathcal{T}_l^{1d}}, \quad \mathcal{T}_l^{(10)} := \overline{\mathcal{T}_{<l}^{1d} \times \mathcal{T}_l^{1d}}, \quad \mathcal{T}_l^{(01)} := \overline{\mathcal{T}_l^{1d} \times \mathcal{T}_{<l}^{1d}},$$

are such that $|\mathcal{T}_0^{(00)}| = 1$, $|\mathcal{T}_l^{(11)}| = |\mathcal{T}_l^{(01)}| = |\mathcal{T}_l^{(10)}| = |\mathcal{T}_l^{1d}|^2 = 2^{2(l-1)}$, and

$$\mathcal{T}_0^{(00)} \cup \bigcup_{l \in \llbracket r \rrbracket} \left(\mathcal{T}_l^{(01)} \cup \mathcal{T}_l^{(11)} \cup \mathcal{T}_l^{(10)} \right) = \llbracket N^2 \rrbracket.$$

Therefore, as illustrated in Fig. 1-left, we can order the columns of Ψ_{idhw} such that, for the 2-D isotropic wavelet levels $\mathcal{T}^{\text{iso}} := \{\mathcal{T}_l^{\text{iso}}\}_{l=0}^r$ defined by

$$\mathcal{T}_0^{\text{iso}} := \mathcal{T}_0^{(00)}, \quad \text{and} \quad \mathcal{T}_l^{\text{iso}} := \mathcal{T}_l^{(01)} \cup \mathcal{T}_l^{(11)} \cup \mathcal{T}_l^{(10)}, \quad l \in \llbracket r \rrbracket_0, \quad (23)$$

we have $\Psi_{\text{idhw}} P_{\mathcal{T}_0^{\text{iso}}}^\top = \Psi_0^{(00)}$, $\Psi_{\text{idhw}} P_{\mathcal{T}_l^{(ab)}}^\top = \Psi_l^{(ab)}$, and $\Psi_{\text{idhw}} P_{\mathcal{T}_l^{\text{iso}}}^\top = [\Psi_l^{(01)}, \Psi_l^{(11)}, \Psi_l^{(10)}]$ for $l \in \llbracket r \rrbracket$ and $(a, b) \in \{0, 1\}^2 \setminus \{(0, 0)\}$.

(Paley-ordered) Hadamard matrix: We now present an important family of orthogonal matrices introduced by J. Hadamard [66], *i.e.*, the Hadamard matrix, that has appeared in various fields, *e.g.*, coding theory [67], harmonic analysis [68], and optics [38]. There exist mainly three constructions of the Hadamard matrix, each with specific row ordering, called ordinary (or Sylvester)-, sequency-, and Paley-ordered Hadamard matrix [69, 70]. In this paper, we focus only on the Paley-ordered Hadamard matrix. But all our results are clearly extendable to the other two constructions after proper reordering (see [47, Chapter 4] for the row ordering).

Given $r \in \mathbb{N}$, the $2^r \times 2^r$ Hadamard matrix [51, 71] $\Phi_{\text{had}} := \mathbf{H}_r \in \{\pm 2^{-r/2}\}^{2^r \times 2^r}$ is defined by

$$\mathbf{H}_r := \frac{1}{\sqrt{2}} \left[\mathbf{H}_{r-1} \otimes \begin{bmatrix} 1 \\ 1 \end{bmatrix}, \mathbf{H}_{r-1} \otimes \begin{bmatrix} 1 \\ -1 \end{bmatrix} \right], \quad \mathbf{H}_0 := [1]. \quad (24)$$

Note that this recurrence relation bears some resemblance with the one of the Haar wavelet basis in (17). Moreover, from (24), we can easily show that Φ_{had} is symmetric, *i.e.*, $\Phi_{\text{had}}^\top = \Phi_{\text{had}}$. The Hadamard transformation of a signal $\mathbf{x} \in \mathbb{C}^N$ with $N = 2^r$ reads $\mathbf{z} = \Phi_{\text{had}}^\top \mathbf{x}$. For 2-D signals, the Hadamard basis is defined by $\Phi_{2\text{had}} := \Phi_{\text{had}} \otimes \Phi_{\text{had}} \in \mathbb{R}^{N^2 \times N^2}$ so that the Hadamard transformation of a matrix $\mathbf{X} \in \mathbb{C}^{N \times N}$ is $\mathbf{Z} = \Phi_{\text{had}}^\top \mathbf{X} \Phi_{\text{had}}$, or equivalently $\text{vec}(\mathbf{Z}) = \Phi_{2\text{had}}^\top \text{vec}(\mathbf{X})$.

Remark 2. Following the definition of $\Phi_{2\text{had}}$, $\mathcal{T}^{\text{aniso}}$, and \mathcal{T}^{iso} and using Lemma. 3 we directly deduce that, for $l_1, l_2 \in \llbracket r \rrbracket_0$ and $l \in \llbracket (r+1)^2 \rrbracket$,

$$P_{\mathcal{T}_l^{\text{aniso}}} \Phi_{2\text{had}}^\top = \left(P_{\mathcal{T}_{l_2}^{1d}} \Phi_{\text{had}}^\top \right) \otimes \left(P_{\mathcal{T}_{l_1}^{1d}} \Phi_{\text{had}}^\top \right), \quad l \xrightarrow{r+1} (l_1 + 1, l_2 + 1),$$

and for $l \in \llbracket r \rrbracket_0$,

$$P_{\mathcal{T}_l^{\text{iso}}} \Phi_{2\text{had}}^\top = \begin{bmatrix} P_{\overline{\mathcal{T}_l^{1d} \times \mathcal{T}_{<l}^{1d}}} (\Phi_{\text{had}} \otimes \Phi_{\text{had}}) \\ P_{\overline{\mathcal{T}_l^{1d} \times \mathcal{T}_l^{1d}}} (\Phi_{\text{had}} \otimes \Phi_{\text{had}}) \\ P_{\overline{\mathcal{T}_{<l}^{1d} \times \mathcal{T}_l^{1d}}} (\Phi_{\text{had}} \otimes \Phi_{\text{had}}) \end{bmatrix} = \begin{bmatrix} (P_{\mathcal{T}_{<l}^{1d}} \Phi_{\text{had}}) \otimes (P_{\mathcal{T}_l^{1d}} \Phi_{\text{had}}) \\ (P_{\mathcal{T}_l^{1d}} \Phi_{\text{had}}) \otimes (P_{\mathcal{T}_l^{1d}} \Phi_{\text{had}}) \\ (P_{\mathcal{T}_l^{1d}} \Phi_{\text{had}}) \otimes (P_{\mathcal{T}_{<l}^{1d}} \Phi_{\text{had}}) \end{bmatrix}.$$

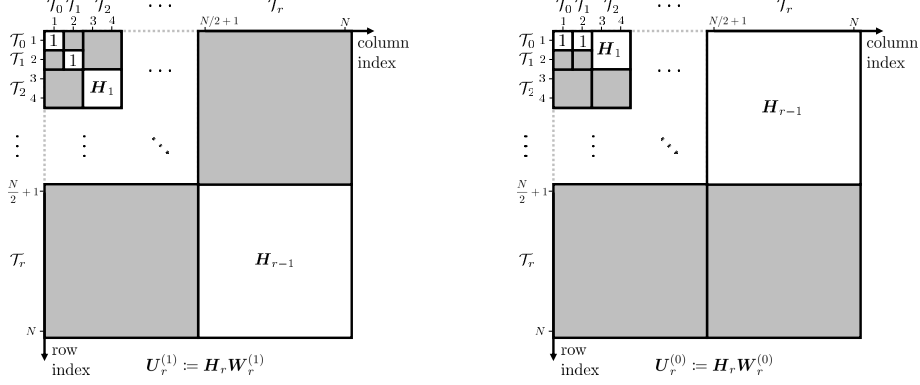


Figure 2: Block structure of the matrices $\mathbf{H}_r \mathbf{W}_r^{(1)}$ (left) and $\mathbf{H}_r \mathbf{W}_r^{(0)}$ (right) where $\mathcal{T}_l = \mathcal{T}_l^{1d}$ for $l \in \llbracket r \rrbracket_0$. Gray color represents zero value.

3.2 Main Results

Equipped with the definitions above, we are now ready to develop our main results. To do so, we need to calculate the local coherence (5), multilevel coherence (10), and relative sparsity (9) for the Hadamard-Haar systems in one and two dimensions. Note that the proofs of this section are all postponed to Sec. 5.

We start with the following crucial proposition; it captures a particular recursive block structure of the Hadamard-Haar matrix obtained by multiplying the 1-D Hadamard and Haar matrices.

Proposition 1. *Given the integer $r \geq 0$ and defining the Hadamard-Haar matrix $\mathbf{U}_r^{(a)} := \mathbf{H}_r^\top \mathbf{W}_r^{(a)}$ for $a \in \{0, 1\}$, we observe that $\mathbf{U}_0^{(1)} = \mathbf{U}_0^{(0)} = [1]$, and for $r \geq 1$,*

$$\mathbf{U}_r^{(1)} = \begin{bmatrix} \mathbf{U}_{r-1}^{(1)} & \mathbf{0} \\ \mathbf{0} & \mathbf{H}_{r-1} \end{bmatrix}, \quad \mathbf{U}_r^{(0)} = \begin{bmatrix} \mathbf{U}_{r-1}^{(0)} & \mathbf{H}_{r-1} \\ \mathbf{0} & \mathbf{0} \end{bmatrix}.$$

In particular, the matrix $\mathbf{U}_r^{(1)}$ is clearly symmetric, and $\mathbf{U}_r^{(1)}$ and $\mathbf{U}_r^{(0)}$ contain the structure illustrated in Fig. 2.

Proof. See Sec. 5.2. □

Remark 3. *In the context of Prop. 1, from the definition of $\mathcal{T}_l = \mathcal{T}_l^{1d}$ in (20) and block structure of $\mathbf{U}_r^{(0)}$ and $\mathbf{U}_r^{(1)}$ unfolded in Fig. 2, we easily deduce the following relations: for $t, l \in \llbracket r \rrbracket_0$, we have*

$$\mathbf{P}_{\mathcal{T}_t} \mathbf{U}_r^{(1)} \mathbf{P}_{\mathcal{T}_l}^\top = \begin{cases} \mathbf{H}_{(t-1)_+}, & \text{if } t = l, \\ \mathbf{0}, & \text{otherwise,} \end{cases} \quad (26a)$$

$$\mathbf{P}_{\mathcal{T}_{<t}} \mathbf{U}_r^{(1)} \mathbf{P}_{\mathcal{T}_l}^\top = \begin{cases} \mathbf{U}_r^{(1)} \mathbf{P}_{\mathcal{T}_l}^\top, & \text{if } t > l, \\ \mathbf{0}, & \text{otherwise,} \end{cases} \quad (26b)$$

$$\mathbf{P}_{\mathcal{T}_t} \mathbf{U}_r^{(0)} \mathbf{P}_{\mathcal{T}_t}^\top = \begin{cases} 1, & \text{if } t = 0, \\ \mathbf{0}, & \text{otherwise,} \end{cases} \quad (26c)$$

$$\mathbf{P}_{\mathcal{T}_{<t}} \mathbf{U}_r^{(0)} \mathbf{P}_{\mathcal{T}_t}^\top = \mathbf{H}_{t-1}, \text{ for } t > 0, \quad (26d)$$

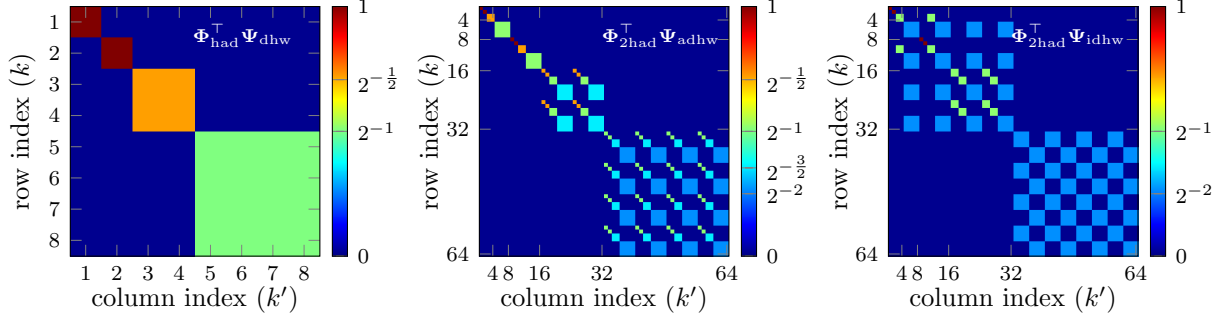


Figure 3: Structure of the matrix $|(\Phi_{\text{had}}^\top \Psi_{\text{dhw}})_{k,k'}|$ (left), $|(\Phi_{2\text{had}}^\top \Psi_{\text{adhw}})_{k,k'}|$ (middle), and $|(\Phi_{2\text{had}}^\top \Psi_{\text{idhw}})_{k,k'}|$ (right) for $N = 8$. We observe that the figure in the middle is the Kronecker product of the matrix on the left with itself. This is actually the consequence of the construction of the 2-D Hadamard matrix and ADHW basis using the Kronecker product.

where $(u)_+ := \max(u, 0)$.

Noting that $|(\mathbf{H}_r)_{k,k'}| = 2^{-r/2}$ for $r \geq 0$ and $k, k' \in \llbracket 2^r \rrbracket$, Fig. 3-left confirms the result in Prop. 1 for $N = 8$.

We now focus on the 2-D Hadamard-Haar systems to extract a similar structure.

Proposition 2. *Given an integer $r \geq 0$, we observe that*

(i) for $t \stackrel{r+1}{\longleftarrow} (t_1 + 1, t_2 + 1)$, $l \stackrel{r+1}{\longleftarrow} (l_1 + 1, l_2 + 1)$, $t_1, t_2, l_1, l_2 \in \llbracket r \rrbracket_0$,

$$\mathbf{P}_{\mathcal{T}_t^{\text{aniso}}} \Phi_{2\text{had}}^\top \Psi_{\text{adhw}} \mathbf{P}_{\mathcal{T}_l^{\text{aniso}}}^\top = \begin{cases} \mathbf{H}_{(t_2-1)_+} \otimes \mathbf{H}_{(t_1-1)_+}, & \text{if } t_1 = l_1, \quad t_2 = l_2, \\ \mathbf{0}, & \text{otherwise,} \end{cases} \quad (27\text{a})$$

(ii) $\mathbf{P}_{\mathcal{T}_0^{\text{iso}}} \Phi_{2\text{had}}^\top \Psi_{\text{idhw}} \mathbf{P}_{\mathcal{T}_0^{\text{iso}}}^\top = 1$, and for $t, l \in \llbracket r \rrbracket_0$ with $(t, l) \neq (0, 0)$,

$$\mathbf{P}_{\mathcal{T}_t^{\text{iso}}} \Phi_{2\text{had}}^\top \Psi_{\text{idhw}} \mathbf{P}_{\mathcal{T}_l^{\text{iso}}}^\top = \begin{cases} \mathbf{I}_3 \otimes (\mathbf{H}_{(t-1)} \otimes \mathbf{H}_{(t-1)}), & \text{if } t = l, \\ \mathbf{0}, & \text{otherwise.} \end{cases} \quad (27\text{b})$$

Proof. See Sec. 5.3. □

Fig. 3-middle and -right depict the structure of the 2-D Hadamard-Haar matrices obtained by multiplying the 2-D Hadamard and Haar matrices. Prop. 2 provides a meaningful expression for those structures. We emphasize that the key aspects in the proof of this proposition is the design of the 2-D isotropic and anisotropic levels, as well as the specific column ordering of the IDHW matrix explained in Sec. 3.1.

The scaling relations in Prop. 1 and Prop. 2 allow us to determine the local and multilevel coherence of the Hadamard-Haar systems; a result that is at the heart of the proofs of Thm. 3 and Thm. 4.

Proposition 3 (Local coherence of Hadamard-Haar systems). *Given integers $r \geq 1$ and $N = 2^r$, the following equalities hold:*

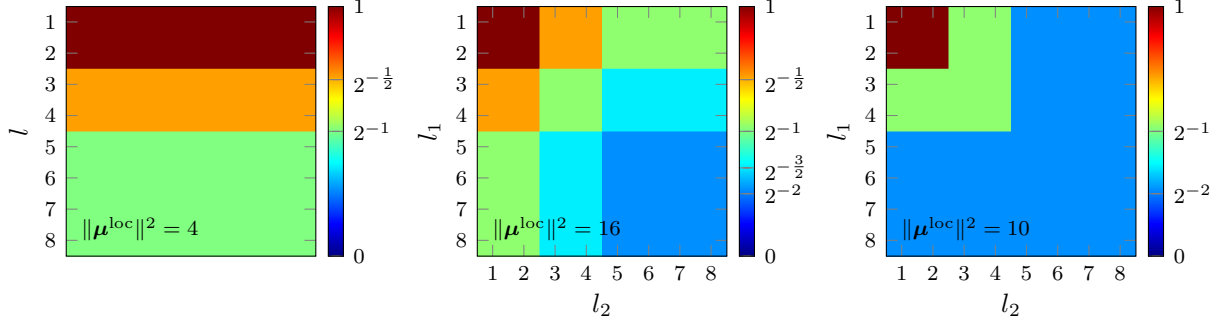


Figure 4: The exact local coherence values for $\mu_l^{\text{loc}}(\Phi_{\text{had}}^\top \Psi_{\text{dhw}})$ (left), $\mu_l^{\text{loc}}(\Phi_{2\text{had}}^\top \Psi_{\text{adhw}})$ (middle), and $\mu_l^{\text{loc}}(\Phi_{2\text{had}}^\top \Psi_{\text{idhw}})$ (right) for $N = 8$, with l_1 and l_2 defined in Prop. 3. The values shown here are equal to the estimated values in Prop. 3. The block structure of these figures, as represented by the constant color areas fits the definition of the wavelet levels, *i.e.*, with 1-D dyadic (left), 2-D anisotropic (middle), and 2-D isotropic (right) levels.

(i) for the 1-D Hadamard-Haar system: for $l \in \llbracket N \rrbracket$,

$$\begin{cases} \mu_l^{\text{loc}}(\Phi_{\text{had}}^\top \Psi_{\text{dhw}}) = \min\left(1, 2^{-\frac{\lfloor \log_2(l-1) \rfloor}{2}}\right), \\ \|\mu^{\text{loc}}(\Phi_{\text{had}}^\top \Psi_{\text{dhw}})\|^2 = \log_2(N) + 1, \end{cases} \quad (28a)$$

(ii) for the 2-D isotropic Hadamard-Haar system: for $l \stackrel{N}{=} (l_1, l_2)$,

$$\begin{cases} \mu_l^{\text{loc}}(\Phi_{2\text{had}}^\top \Psi_{\text{idhw}}) = \min\left(1, 2^{-\lfloor \log_2(\max(l_1, l_2) - 1) \rfloor}\right), \\ \|\mu^{\text{loc}}(\Phi_{2\text{had}}^\top \Psi_{\text{idhw}})\|^2 = 3 \log_2(N) + 1, \end{cases} \quad (28b)$$

(iii) for the 2-D anisotropic Hadamard-Haar system: for $l \stackrel{N}{=} (l_1, l_2)$,

$$\begin{cases} \mu_l^{\text{loc}}(\Phi_{2\text{had}}^\top \Psi_{\text{adhw}}) = \min\left(1, 2^{-\frac{\lfloor \log_2(l_1-1) \rfloor}{2}}\right) \cdot \min\left(1, 2^{-\frac{\lfloor \log_2(l_2-1) \rfloor}{2}}\right), \\ \|\mu^{\text{loc}}(\Phi_{2\text{had}}^\top \Psi_{\text{adhw}})\|^2 = (\log_2(N) + 1)^2. \end{cases} \quad (28c)$$

Proof. See Sec. 5.4. □

The exact values of the local coherence are illustrated in Fig.4 for $N = 8$. We thus observe that those values are well-controlled in Prop. 3, while the global coherence of the Hadamard-Haar systems is equal to one. Since the value of the local coherence is closed-form in all the three cases considered in Prop. 3, following the argument of Thm. 1, we can set the upper bounds κ_l to μ_l^{loc} to characterize the associated systems in the following theorem.

Theorem 3 (Uniform guarantee for Hadamard-Haar systems). *Fix $N = 2^r$ for some integer $r \in \mathbb{N}$. We provide below, for three Hadamard-Haar systems (Φ, Ψ) in one and two dimensions, the sample-complexity bound and sampling pmf ensuring (6) and (7) in Thm. 1:*

(i) for the 1-D Hadamard-Haar system: $\Phi = \Phi_{\text{had}} \in \mathbb{R}^{N \times N}$, $\Psi = \Psi_{\text{dhw}} \in \mathbb{R}^{N \times N}$,

$$M \gtrsim K \log(N) \log(\epsilon^{-1}), \text{ and } \eta(l) = \frac{\min(1, 2^{-\lfloor \log_2(l-1) \rfloor})}{\log_2(N) + 1}, \quad l \in \llbracket N \rrbracket, \quad (29a)$$

(ii) for the 2-D isotropic Hadamard-Haar system: $\Phi = \Phi_{2\text{had}} \in \mathbb{R}^{N^2 \times N^2}$, $\Psi = \Psi_{\text{idhw}} \in \mathbb{R}^{N^2 \times N^2}$,

$$M \gtrsim K \log(N) \log(\epsilon^{-1}), \text{ and } \eta(l) = \frac{\min(1, 2^{-2 \lfloor \log_2(\max(l_1, l_2) - 1) \rfloor})}{3 \log_2(N) + 1}, \quad l \stackrel{N}{=} (l_1, l_2), \quad (29b)$$

(iii) for the 2-D anisotropic Hadamard-Haar system: $\Phi = \Phi_{2\text{had}} \in \mathbb{R}^{N^2 \times N^2}$, $\Psi = \Psi_{\text{adhw}} \in \mathbb{R}^{N^2 \times N^2}$,

$$M \gtrsim K \log^2(N) \log(\epsilon^{-1}), \text{ and } \eta(l) = \frac{\min(1, 2^{-\lfloor \log_2(l_1 - 1) \rfloor}) \cdot \min(1, 2^{-\lfloor \log_2(l_2 - 1) \rfloor})}{(\log_2(N) + 1)^2}, \quad l \stackrel{N}{=} (l_1, l_2). \quad (29c)$$

According to this theorem, the optimal sampling pmf $\eta(l)$ is a non-increasing function of l . Since $\eta(l) \propto (\mu_l^{\text{loc}})^2$, (up to a normalization factor $\|\boldsymbol{\mu}^{\text{loc}}\|^2$) the values in Fig. 4 indicate the decay behavior of the sampling pmf. In all the Hadamard-Haar systems, the total number of measurements M is on the order of global sparsity K . However, following the computation of the local coherence values in Prop. 3, it could be noticed that the use of the UDS strategy gives $M \gtrsim NK \log(\epsilon^{-1}) \log^\alpha(N)$ for some $\alpha \in \{1, 2\}$. Moreover, the required number of measurements in (29c) is larger than the one in (29b) by a $\log(N)$ factor: for those signals that have the same sparsity in IDHW and ADHW bases, *i.e.*, $\sigma_K(\Psi_{\text{idhw}}^\top \mathbf{x})_1 \approx \sigma_K(\Psi_{\text{adhw}}^\top \mathbf{x})_1$, by considering IDHW basis as the sparsity basis we would require smaller number of measurements for signal recovery.

We now turn our attention to the non-uniform guarantee. Following the sample-complexity bounds (13) and (11), for a fixed signal and fixed sensing and sparsity bases, the efficiency of the MDS scheme relies on (i) a suitable partitioning of the sampling and sparsity domains and (ii) the ability to estimate the accurate multilevel coherence and relative sparsity values.

One way to design the sampling and sparsity levels is to leverage the structure of the Hadamard-Haar systems observed in Prop. 1 and Prop. 2. To visualize those structure, one can properly permute the columns and the rows of the matrices in Fig. 3 according to specific wavelet levels, *e.g.*, the 1-D dyadic, 2-D isotropic, or 2-D anisotropic, and obtain the matrices in Fig. 5. Each white rectangle in Fig. 5 centered at the index (t, l) corresponds to a single partition. Note that the horizontal and vertical axis in Fig. 5 denotes the sparsity and sampling level index, respectively; while the axis in Fig. 3 represent the column and row indices. The observed structures in Fig. 5, specially the ones related to the ADHW and IDHW bases, confirms the statements of Prop. 1 and Prop. 2. With these structures in mind, we can now compute the following values for multilevel coherence and relative sparsity in different Hadamard-Haar systems.

Proposition 4 (Multilevel coherence and relative sparsity of Hadamard-Haar systems). *Fix integers r and $N = 2^r$. We consider the levels \mathcal{T}^{1d} , \mathcal{T}^{iso} , and $\mathcal{T}^{\text{aniso}}$ defined above and, for each of them, a vector \mathbf{k} whose size equals the number of levels. Then, the following holds:*

(i) for the 1-D Hadamard-Haar system: for $t, l \in \llbracket r \rrbracket_0$,

$$\begin{cases} \mu_{t,l}^{\mathcal{T}^{\text{1d}}, \mathcal{T}^{\text{1d}}}(\Phi_{\text{had}}^\top \Psi_{\text{dhw}}) = 2^{-(t-1)_+} \cdot \delta_{t,l}, \\ K_t^{\mathcal{T}^{\text{1d}}, \mathcal{T}^{\text{1d}}}(\Phi_{\text{had}}^\top \Psi_{\text{dhw}}, \mathbf{k}) \leq k_t, \end{cases} \quad (30a)$$

(ii) for the 2-D isotropic Hadamard-Haar system: for $t, l \in \llbracket r \rrbracket_0$,

$$\begin{cases} \mu_{t,l}^{\mathcal{T}^{\text{iso}}, \mathcal{T}^{\text{iso}}}(\Phi_{2\text{had}}^\top \Psi_{\text{idhw}}) = 2^{-2(t-1)_+} \cdot \delta_{t,l}, \\ K_t^{\mathcal{T}^{\text{iso}}, \mathcal{T}^{\text{iso}}}(\Phi_{2\text{had}}^\top \Psi_{\text{idhw}}, \mathbf{k}) \leq k_t, \end{cases} \quad (30b)$$

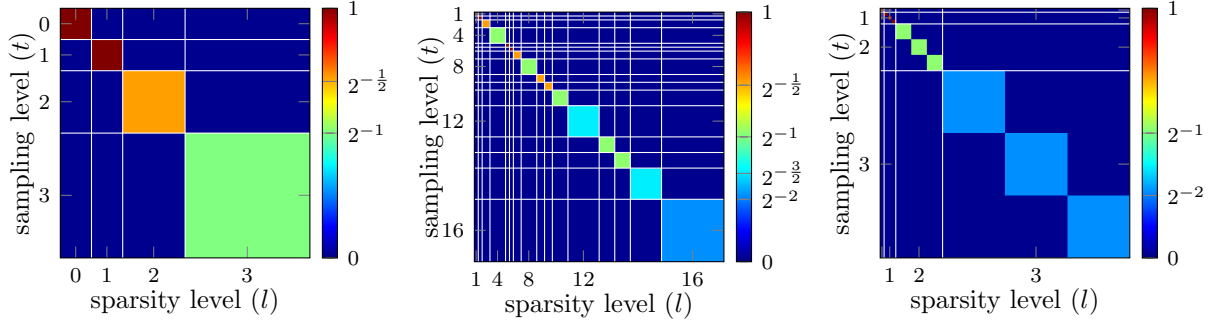


Figure 5: Rearrangement of the rows and columns of the matrices shown in Fig. 3 with respect to the sampling and sparsity levels. Each white rectangle centered at (t, l) corresponds to the $(t, l)^{\text{th}}$ block, *i.e.*, $\mathbf{P}_{\mathcal{T}_t^{1d}} \Phi_{\text{had}}^\top \Psi_{\text{dhw}} \mathbf{P}_{\mathcal{T}_l^{1d}}^\top$ (left), $\mathbf{P}_{\mathcal{T}_t^{\text{aniso}}} \Phi_{2\text{had}}^\top \Psi_{\text{adhw}} \mathbf{P}_{\mathcal{T}_l^{\text{aniso}}}^\top$ (middle), and $\mathbf{P}_{\mathcal{T}_t^{\text{iso}}} \Phi_{2\text{had}}^\top \Psi_{\text{idhw}} \mathbf{P}_{\mathcal{T}_l^{\text{iso}}}^\top$ (right).

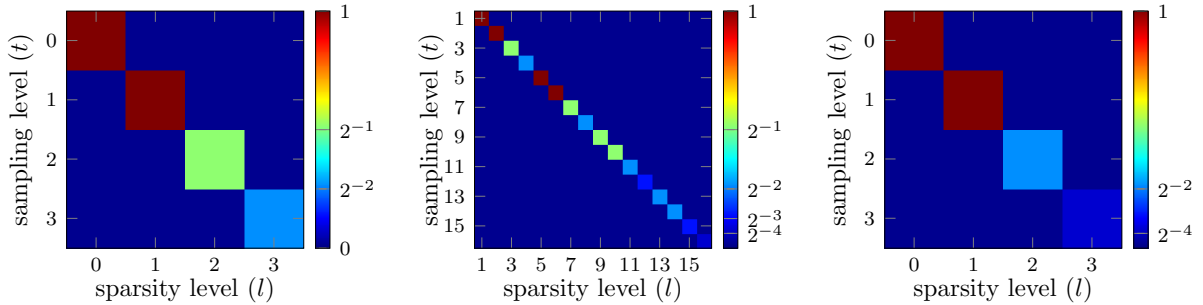


Figure 6: The exact multilevel coherence values for Hadamard-Haar systems with $N = 8$: (left) $\mu_{t,l}^{\mathcal{T}^{1d}, \mathcal{T}^{1d}}(\Phi_{\text{had}}^\top \Psi_{\text{dhw}})$, (middle) $\mu_{t,l}^{\mathcal{T}^{\text{iso}}, \mathcal{T}^{\text{iso}}}(\Phi_{2\text{had}}^\top \Psi_{\text{adhw}})$, and (right) $\mu_{t,l}^{\mathcal{T}^{\text{iso}}, \mathcal{T}^{\text{iso}}}(\Phi_{2\text{had}}^\top \Psi_{\text{idhw}})$. The multilevel coherence values in this figure confirm our estimations in Prop. 4.

(iii) for the 2-D anisotropic Hadamard-Haar system: for $t \stackrel{r+1}{\iff} (t_1 + 1, t_2 + 1)$, $l \stackrel{r+1}{\iff} (l_1 + 1, l_2 + 1)$,

$$\begin{cases} \mu_{t,l}^{\mathcal{T}^{\text{aniso}}, \mathcal{T}^{\text{aniso}}}(\Phi_{2\text{had}}^\top \Psi_{\text{adhw}}) = 2^{-(t_1-1)_+} \cdot 2^{-(t_2-1)_+} \cdot \delta_{t_1, l_1} \cdot \delta_{t_2, l_2}, \\ K_t^{\mathcal{T}^{\text{aniso}}, \mathcal{T}^{\text{aniso}}}(\Phi_{2\text{had}}^\top \Psi_{\text{adhw}}, \mathbf{k}) \leq k_t, \end{cases} \quad (30c)$$

where the relative sparsity $K_t^{\mathcal{W}, \mathcal{S}}$ and the multilevel coherence $\mu_{t,l}^{\mathcal{W}, \mathcal{S}}$ are defined in (9) and (10), respectively, and where $\delta_{t,l}$ is a Kronecker function, *i.e.*, $\delta_{k,l} = 1$ if $t = l$ (and zero, otherwise).

Proof. See Sec. 5.5. □

According to Prop. 4, the multilevel coherence is an exponentially-decreasing function of the level index (see also Fig. 6 for an illustration of the multilevel coherence for $N = 8$). Moreover, as an advantage of our sampling and sparsity levels design, the multilevel coherence of the Hadamard-Haar systems at level (t, l) vanishes when $t \neq l$ and thus, the sample-complexity bounds (13) and (11) become

$$\begin{aligned} m_t &\gtrsim |\mathcal{W}_t| \mu_{t,t}^{\mathcal{W}, \mathcal{S}}(\Phi^\top \Psi) k_t \log(K\epsilon^{-1}) \log(N), \\ 1 &\gtrsim \left(\frac{|\mathcal{W}_t|}{\hat{m}_t} - 1 \right) \mu_{t,l}^{\mathcal{W}, \mathcal{S}}(\Phi^\top \Psi) K_l^{\mathcal{W}, \mathcal{S}}(\Phi^\top \Psi, \mathbf{k}). \end{aligned}$$

If we ignore the second sample-complexity bound, the first bound relates the number of measurements m_t at level t to the sparsity value k_t at the same level t (and not to the sparsity values at the other levels). This is exactly as one expects when the matrix $\Phi^\top \Psi$ is block-diagonal (see [12, Sec. 4.2.1] for more insights) and an application of the sample-complexity bound (3) on every block gives the sufficient conditions on the number of measurements.

We are now ready to combine the proposition above with Thm. 2 and present the following non-uniform recovery guarantees of Hadamard-Haar systems.

Theorem 4 (Non-uniform guarantee for Hadamard-Haar systems). *Given $N = 2^r$ for some integer $r \in \mathbb{N}$, if we fix*

$$m_t \gtrsim k_t \log(K\epsilon^{-1}) \log(N) \quad (31)$$

with either:

(i) for the 1-D Hadamard-Haar system:

$$t \in \llbracket r \rrbracket_0, \Phi = \Phi_{\text{had}} \in \mathbb{R}^{N \times N}, \Psi = \Psi_{\text{dhw}} \in \mathbb{R}^{N \times N}, \mathcal{W} = \mathcal{T} = \mathcal{T}^{1\text{d}};$$

(ii) for the 2-D isotropic Hadamard-Haar system:

$$t \in \llbracket r \rrbracket_0, \Phi = \Phi_{2\text{had}} \in \mathbb{R}^{N^2 \times N^2}, \Psi = \Psi_{\text{idhw}} \in \mathbb{R}^{N^2 \times N^2}, \mathcal{W} = \mathcal{T} = \mathcal{T}^{\text{iso}};$$

(iii) for the 2-D anisotropic Hadamard-Haar system:

$$t \in \llbracket (r+1)^2 \rrbracket, \Phi = \Phi_{2\text{had}} \in \mathbb{R}^{N^2 \times N^2}, \Psi = \Psi_{\text{adhw}} \in \mathbb{R}^{N^2 \times N^2}, \mathcal{W} = \mathcal{T} = \mathcal{T}^{\text{aniso}};$$

then (13) and (11) in Thm. 2 are satisfied.

Proof. See Sec. 5.6. □

It is worth mentioning that Thm. 4 provides the tightest sample-complexity bounds, since the multilevel coherence values that lead to these estimates are accurately computed in Prop. 5.5. We observe in Thm. 4 that the local number of measurements m_t for the covered Hadamard-Haar systems is on the order of the corresponding local sparsity k_t . A similar observation has recently been made for the infinite-dimensional Hadamard-Haar system in [25, Thm. 4.13]. Unlike the observation in (31), for an arbitrary orthonormal wavelet basis the local number of measurements m_t scales as a linear combination of the local sparsities (see in [56] or [49, Thm. 5.8]), which is due to the fact that the Hadamard-wavelet system is not exactly block-diagonal.

Remark 4. *One can question how to set the local number of measurements m_t given the local sparsity values k_t and the total number of measurements M . We provide an approach for the 1-D signal recovery problem that is easily extendable to the 2-D cases. The idea here is based on the fact that the local number of measurements in (31) can be written as $m_t = Ck_t$ for $t \in \llbracket r \rrbracket_0$ with $C > 0$ independent of t and k_t . Therefore, the total number of measurements is $M = \sum_t m_t = CK$ where K is the total sparsity value. Therefore, up to a rounding error, the local number of measurements reads*

$$m_t = \frac{M}{K} k_t, \quad t \in \llbracket r \rrbracket_0.$$

4 Numerical results

In this section we carry out several simulations to verify the obtained theoretical results in Thm. 3 and Thm. 4. In the first set of simulations we address the problem of 1-D signal recovery from subsampled Hadamard measurements and later we focus on the 2-D signal recovery problem, which is associated with single pixel imaging application of CS.

The general setup of the simulations is as follows. Given a ground truth signal $\mathbf{x} \in \mathbb{C}^N$ we follow the sensing model (1) for some dimensions and sensing bases to be specified later, where we suppose the noise components $n_l \sim_{\text{i.i.d.}} \mathcal{N}(0, \sigma)$ and σ is fixed with respect to the desired Signal-to-Noise Ratio (SNR) $:= 20 \log_{10}(\|\mathbf{x}\|/(\sigma\sqrt{N}))$ in dB. For all the experiments we report the Signal-to-Reconstruction Error (SRE) in dB, *i.e.*,

$$\text{SRE} := 20 \log_{10} \mathbb{E}_e \|\mathbf{x}\| / \|\mathbf{x} - \hat{\mathbf{x}}\|,$$

where \mathbb{E}_e is the empirical mean over several trials of the sensing context (as specified in the text). In this section the term ‘‘VDS’’ (or ‘‘MDS’’) implies the sampling strategies defined in Thm. 3 (resp. Thm. 4). For the MDS scheme we respect the approach described in Remark 4. We consider two algorithms for signal reconstruction: (i) CS reconstruction, that refers to the ℓ_1 minimization problem (14) or (8) (depending on the recovery guarantee type) for some sparsity basis to be specified later; and (ii) Minimal Energy (ME) reconstruction [72], which corresponds to applying the right pseudo-inverse of Φ to the measurement vector. CS reconstructions (14) and (8) are performed with the Spectral Projected Gradient for ℓ_1 minimization (SPGL1) [73, 74]. In our experiments, the parameter ε in (8) (and (14)) is set to the oracle value of $\|\mathbf{D}\mathbf{n}\|$ (resp. $\|\mathbf{n}\|$). Matrices and operators are implemented using the Spot toolbox [75].

The MDS schemes in Thm. 4 require to set the values of the local sparsity parameter k_l . For these simulations, when the signal of interest is not exactly sparse we perform the following procedure that is proposed by Adcock *et al.* in [12, Eq. 2.8] and used in [29]: (i) given a parameter $\rho \in (0, 1]$ and a signal $\mathbf{x} \in \mathbb{C}^N$ we first compute the vector of coefficients $\mathbf{s} \in \mathbb{C}^N$ in the sparsity basis Ψ , *i.e.*, $\mathbf{s} = \Psi^\top \mathbf{x}$; (ii) the effective global sparsity value K is then computed such that after applying the hard thresholding operator \mathcal{H}_K to \mathbf{s} , the ratio of the energy that is preserved by K coefficients equals ρ , mathematically,

$$K = K(\rho) = \min\{n : \|\mathcal{H}_n(\mathbf{s})\| / \|\mathbf{s}\| \geq \rho\},$$

where we set $\rho = 0.995$ in all the experiments here ; (iii) we finally compute the effective local sparsity values by simply localizing the number of non-zero coefficients of the hard thresholded signal $\mathcal{H}_K(\mathbf{s})$, *i.e.*, for all l

$$k_l = k_l(\rho) = |\text{supp}(\mathbf{P}_{S_l} \mathcal{H}_K(\rho)(\mathbf{s}))|.$$

Note that this procedure does not sparsify the signal \mathbf{x} in the basis Ψ , as it is only used to estimate the parameters k_l .

4.1 1-D signal recovery

We here examine the VDS and MDS schemes defined in Thm. 3 and Thm. 4 by comparing their SRE values with the one achieved by UDS scheme for different signals. In this part, the sensing and sparsity bases are set to the 1-D Hadamard and DHW bases, respectively, and the signals are

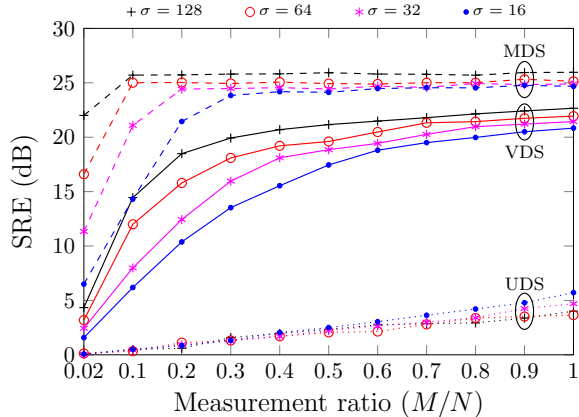


Figure 7: The reconstruction performance comparison of the proposed MDS and VDS schemes with the traditional UDS scheme.

recovered via only CS reconstruction. In the first simulation, a Gaussian-shape signal $\mathbf{x} \in \mathbb{R}^N$ of size $N = 512$, *i.e.*,

$$x_i = \frac{1}{\sigma\sqrt{2\pi}} \exp\left(-\frac{(i-i_0)^2}{2\sigma^2}\right), \quad \forall i \in \llbracket N \rrbracket,$$

is generated as the ground truth. The variables i_0 and σ determine the center and the width of the Gaussian curve. Essentially, by increasing σ the coefficients of the signal in Haar wavelet domain become sparser. The variable $\sigma \in \{16, 32, 64, 128\}$ and the parameter i_0 is generated uniformly at random in the range $[\sigma, N - \sigma]$. We set the variance of the noise to read an SNR of 20 dB. Fig. 7 displays the reconstruction quality of the generated signals as a function of the measurement ratio (M/N) for different values of σ and sampling strategies (UDS, VDS, and MDS). Each point of the curves in Fig. 7 is an average of 100 trials (*i.e.*, over random generation of the noise, subsampling set Ω , and parameter i_0).

In the simulations here with MDS scheme, the effective local sparsities $k_l(\rho)$ are fixed for each value of σ a priori. In particular, given σ we first generate 100 Gaussian-shape signals (different from the ones to be recovered) whose locations i_0 are selected uniformly at random; and then compute their effective local sparsities as prescribed above. Finally, we consider the worst local sparsity values k_l with $l \in \llbracket r \rrbracket$ over all 100 trials for designing our MDS scheme. This approach gives a near-optimal MDS strategy, yet it is of practical interest where the true values of the local sparsity are not accessible.

From Fig. 7, we can make the following observations: (*i*) by increasing the value of σ the signal becomes sparser in the Haar domain, and thus, all reconstructions yield better SRE values; (*ii*) the UDS scheme yields a poor reconstruction quality; this is aligned with the large value of the global coherence between the Hadamard and Haar bases, which drives the UDS sample-complexity in (3); (*iii*) the VDS scheme provides a stable and robust signal recovery (with respect to the change of sparsity and noise level); (*iv*) the SRE of the Hadamard-Haar system is further increased by using the MDS scheme, since it adjusts the sampling strategy to the sparsity structure of the signal; (*v*) although the MDS scheme here is not designed based on the ground truth signal, the dashed lines show significant SRE improvement compared to the VDS strategy.

In Fig. 8, we apply similar tests on four other functions, *i.e.*, the “Blocks”, “Bumps”, “Heav-iSine”, and “Doppler” signals taken from [76]. These signals display various behaviors, hence

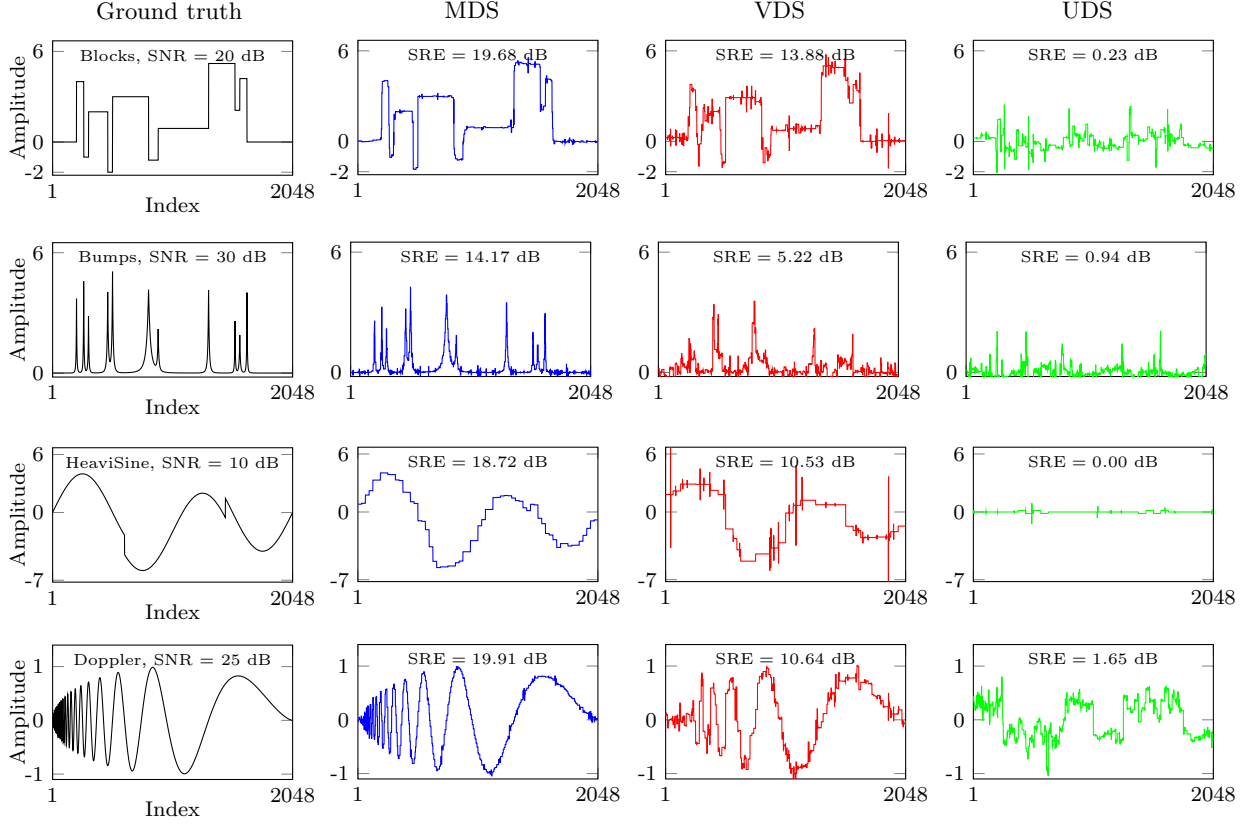


Figure 8: Recovering four special 1-D signals from 20% Hadamard measurements.

allowing us to test our scheme in a broader context. They are generated by evenly sampling the continuous functions specified in [76] over $N = 2048$ samples.

The reconstructed signals from 20% subsampled Hadamard measurements using MDS, VDS, and UDS schemes are displayed in Fig. 8. As can be seen, the UDS strategy does not allow signal recovery. Note that these signals (except the Blocks signal) are not well-compressible in the Haar basis. As a consequence, most reconstructions have blocky artifacts and the VDS scheme does not provide a high quality reconstruction. The MDS scheme, which leverages the local compressibility of the signal, achieves a much higher reconstruction quality in all examples.

4.2 2-D signal recovery

We now test the performance of the proposed VDS and MDS schemes in an imaging context. We generate synthetic Shepp-Logan phantom images [77] of size $N \times N$ with $N = 2^r$ and $r \in \{7, \dots, 11\}$ as the ground truth. The variance of the noise amounts to an SNR of 20 dB. Fig. 9 illustrates the SRE values as a function of the measurement ratio (M/N^2) for different resolutions N , sampling strategies (UDS, VDS, and MDS), sparsity bases (IDHW and ADHW), and recovery algorithms (CS and ME). The results are averaged over 10 trials (*i.e.*, over the random generation of both the noise and random selection of the subsampling set Ω according to the sampling strategy). We note that in Fig. 9 and in the UDS and VDS cases, since there are repeated indices in the subsampled set Ω , even for $M/N^2 = 1$, we cannot reach the recovery quality of fully-sampled (or

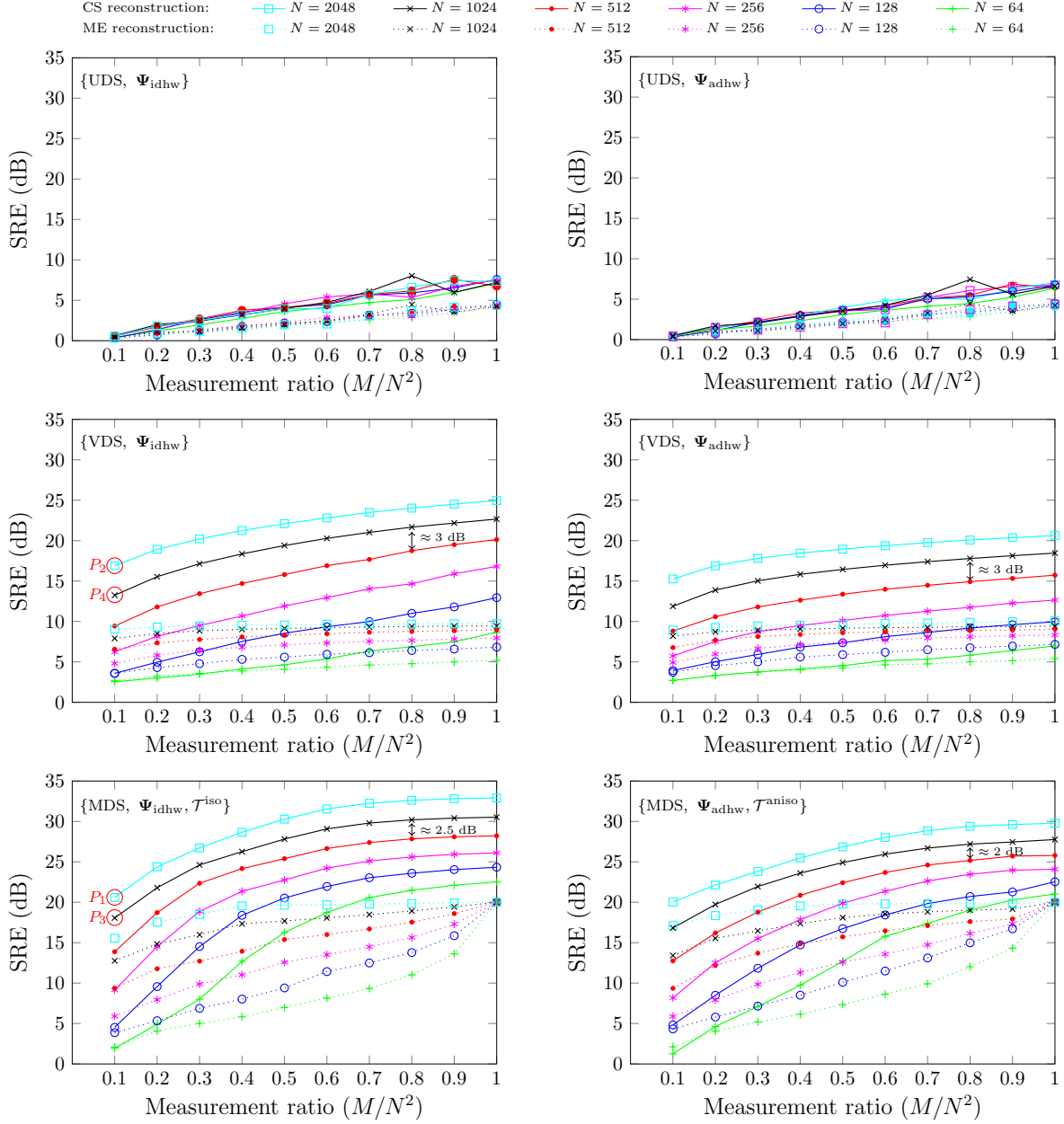


Figure 9: The SRE of phantom image recovery from subsampled Hadamard measurements.

Nyquist) Hadamard measurements. On the contrary, since MDS scheme does not allow repeated indices, the recovery quality of the Nyquist Hadamard-Haar system happens when $M/N^2 = 1$. Not surprisingly, ME reconstruction yields $\text{SRE} = \text{SNR} = 20$ dB when the Hadamard measurements are fully-sampled. Fig. 10 displays the global and local sparsity of the phantom images of different sizes in 2-D Haar wavelet basis. On the left, the sorted coefficients in IDHW and ADHW bases are plotted versus the normalized index axis. Fig. 10-right shows an experiment in which we computed the local sparsity ratios for the phantom image of different sizes using IDHW sparsity basis.

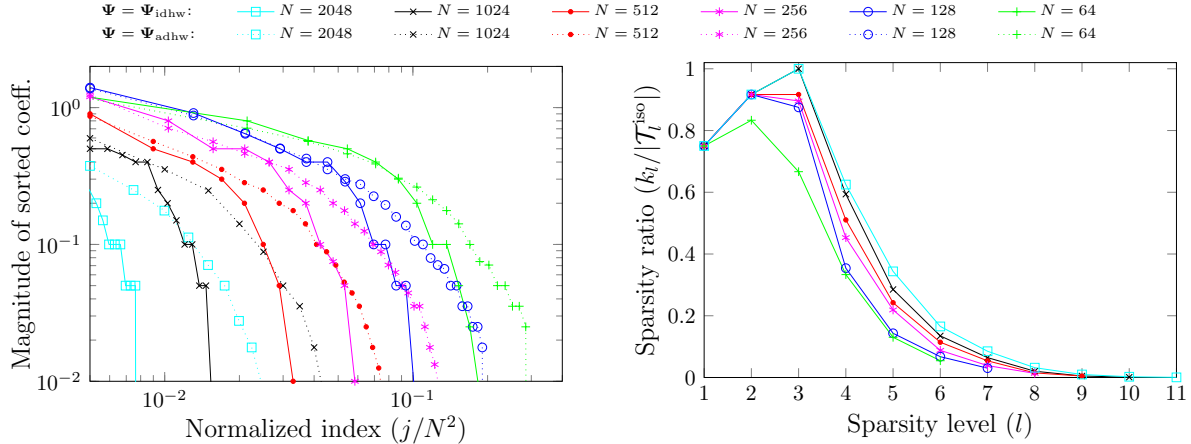


Figure 10: Global (left) and local (right) sparsity of the phantom image in 2-D Haar wavelet basis. On the right figure, in order to obtain meaningful curves we assumed $\mathcal{T}_0^{\text{iso}} = \emptyset$ and $\mathcal{T}_1^{\text{iso}} = \{1, 2\}$.

From Fig. 9 and Fig. 10 we can do the following observations. First, similar to the 1-D signal recovery, the UDS scheme performs poorly. Second, the CS reconstruction always outperforms the ME reconstruction, as the latter does not take into account the sparsity prior information. Third, by increasing the resolution of the signal (or the size of the problem) one can obtain a higher SRE value (up to 3 dB), regardless of the CS or ME reconstruction method. Essentially, by going higher in resolution the signal becomes (asymptotically) sparser in the wavelet domain, as represented in Fig. 10-left. In this figure, the decay rate of the curves increases as N grows. As already stressed in, *e.g.*, [5], the MDS scheme is thus expected to express its efficacy in high-dimensional applications. Fourth, the IDHW basis yields better SRE values in comparison to the ADHW basis because the phantom image is more compressible in the IDHW basis. Concretely, by comparing the solid and dotted lines in Fig. 10-left, we conclude that the phantom image reaches higher compressibility in the IDHW basis, which further increases the quality of the signal recovery. Fifth, the MDS scheme is resolution dependent: following the sample-complexity bounds in Thm. 4, the values in Fig. 10-right determine the required number of measurements at each level. Finally, since the MDS scheme leverages the sparsity structure of the signal, it outperforms the VDS scheme in the sense of recovery quality.

An example of the reconstructed images in the simulation above, marked by points P_1, P_2, P_3 , and P_4 , is depicted in Fig. 11. In this figure we notice the effect of the resolution on the MDS strategy and on the image recovery quality.

5 Proofs

We now turn our attention to the proofs of the main results. We present first a few auxiliary lemmas used later in this section.

Lemma 3. *Let $\mathbf{u} \in \mathbb{C}^N$, $\mathbf{u}' \in \mathbb{C}^{N'}$, and $\mathbf{v} = \mathbf{u}' \otimes \mathbf{u} \in \mathbb{C}^{\bar{N}}$ with $\bar{N} = NN'$. For two sets $\mathcal{S} \subset \llbracket N \rrbracket$ and $\mathcal{S}' \subset \llbracket N' \rrbracket$, and $\mathcal{S} = \mathcal{S} \times \mathcal{S}'$, we have*

$$\mathbf{P}_{\bar{\mathcal{S}}} \mathbf{v} = (\mathbf{P}_{\mathcal{S}'} \mathbf{u}') \otimes (\mathbf{P}_{\mathcal{S}} \mathbf{u}). \quad (32)$$

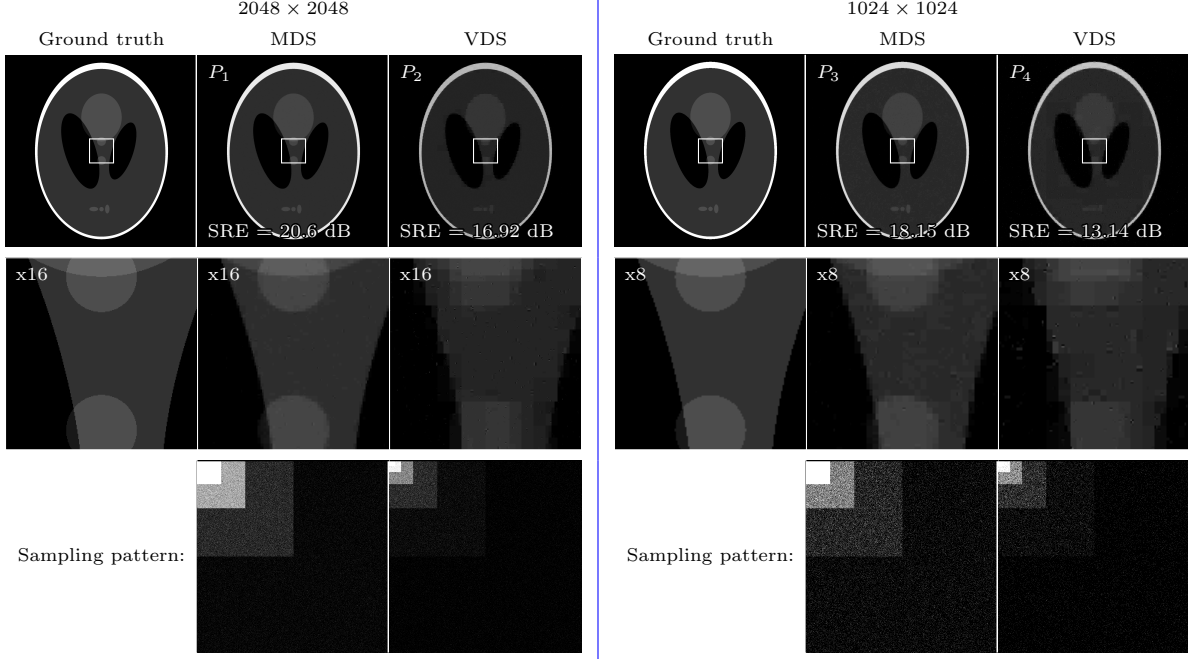


Figure 11: An example of the reconstructed images from 10% of the Hadamard measurements. These images correspond to the points P_1, P_2, P_3 , and P_4 in Fig. 9. Superior quality of the CS reconstruction is obvious both visually and quantitatively. We also recall the repetition in the selected indices in VDS scheme which results in less white points in the sampling pattern.

Proof. Defining $\mathbf{e}_i := (\mathbf{I}_N)_i$, $\mathbf{e}'_j := (\mathbf{I}_{N'})_j$, and $\bar{\mathbf{e}}_l := (\mathbf{I}_{\bar{N}})_l$, we first note that

$$\mathbf{u}' \otimes \mathbf{u} = \sum_{i=1}^{N_1} \sum_{j=1}^{N_2} u_i u'_j (\mathbf{e}'_j \otimes \mathbf{e}_i).$$

Therefore,

$$\begin{aligned} \mathbf{P}_{\bar{S}} \mathbf{v} &= \sum_{l \in \bar{S}} \mathbf{v}_l \bar{\mathbf{e}}_l = \sum_{(i,j) \in \mathcal{S}} u_i u'_j (\mathbf{e}'_j \otimes \mathbf{e}_i) = \sum_{i \in \mathcal{S}} u_i \left(\sum_{j \in \mathcal{S}'} u'_j \mathbf{e}'_j \right) \otimes \mathbf{e}_i \\ &= \sum_{i \in \mathcal{S}} u_i ((\mathbf{P}_{\mathcal{S}'} \mathbf{u}') \otimes \mathbf{e}_i) = (\mathbf{P}_{\mathcal{S}'} \mathbf{u}') \otimes \left(\sum_{i \in \mathcal{S}} u_i \mathbf{e}_i \right) = (\mathbf{P}_{\mathcal{S}'} \mathbf{u}') \otimes (\mathbf{P}_{\mathcal{S}} \mathbf{u}), \end{aligned}$$

where in the first line we used the fact that $u_l = u_i u_j$ and $\bar{\mathbf{e}}_l = \mathbf{e}'_j \otimes \mathbf{e}_i$ for $l \xleftrightarrow{N_1, N_2} (i, j)$. \square

Lemma 4. For $\mathbf{A} \in \mathbb{C}^{M \times N}$ and $\mathbf{B} \in \mathbb{C}^{P \times Q}$, we have

$$\mu(\mathbf{A} \otimes \mathbf{B}) = \mu(\mathbf{A}) \cdot \mu(\mathbf{B}), \quad (33a)$$

$$\mu_l^{\text{loc}}(\mathbf{A} \otimes \mathbf{B}) = \mu_{l_1}^{\text{loc}}(\mathbf{B}) \cdot \mu_{l_2}^{\text{loc}}(\mathbf{A}), \text{ with } l \xleftrightarrow{P, M} (l_1, l_2). \quad (33b)$$

Proof. From the definition of coherence in (4),

$$\mu(\mathbf{A} \otimes \mathbf{B}) = \max_{i,j} |(\mathbf{A} \otimes \mathbf{B})_{i,j}| = \max_{i_1, j_1} |a_{i_1, j_1}| \cdot \max_{i_2, j_2} |b_{i_2, j_2}| = \mu(\mathbf{A}) \cdot \mu(\mathbf{B}).$$

For the second relation, following the definition of the local coherence in (5), we find

$$\mu_l^{\text{loc}}(\mathbf{A} \otimes \mathbf{B}) = \max_j |(\mathbf{a}_{l_2} \otimes \mathbf{b}_{l_1})_j| = \max_{j_1, j_2} |a_{l_2, j_2} \cdot b_{l_1, j_1}| = \max_{j_2} |a_{l_2, j_2}| \cdot \max_{j_1} |b_{l_1, j_1}|,$$

where we used the relation $j \xleftrightarrow{Q, N} (j_1, j_2)$. \square

5.1 Proof of Lemma 2

Below, to get simpler notation, we write \mathcal{T}_l instead of \mathcal{T}_l^{1d} . We first note from (17) and (19) that $\mathbf{W}^{(a)} \mathbf{P}_{\mathcal{T}_0}^\top = \mathbf{1}_{2^r}$, since $\mathbf{W}_0^{(a)} = [1]$, for $a \in \{0, 1\}$. Since $\mathcal{T}_l \subset \mathcal{T}_{<l+1}$ and $\bar{\mathbf{P}}_{\mathcal{T}_{<l+1}} = \mathbf{P}_{\mathcal{T}_{<l+1}}^\top \mathbf{P}_{\mathcal{T}_{<l+1}}$, we have $\mathbf{P}_{\mathcal{T}_l} \bar{\mathbf{P}}_{\mathcal{T}_{<l+1}} = \mathbf{P}_{\mathcal{T}_l}$ and using Lemma 5 proved below we have

$$\mathbf{W}_r^{(a)} \mathbf{P}_{\mathcal{T}_l}^\top = \mathbf{W}_r^{(a)} \bar{\mathbf{P}}_{\mathcal{T}_{<l+1}}^\top \mathbf{P}_{\mathcal{T}_l}^\top = 2^{\frac{l-r}{2}} \left[\mathbf{W}_l^{(a)} \otimes \mathbf{1}_{2^{r-l}}, \mathbf{0} \right] \mathbf{P}_{\mathcal{T}_l}^\top. \quad (34)$$

Inserting the recursive formulation of $\mathbf{W}_r^{(1)}$ and $\mathbf{W}_r^{(0)}$ in (17) and (19), respectively, in (34), using $(\mathbf{A} \otimes \mathbf{B}) \otimes \mathbf{C} = \mathbf{A} \otimes (\mathbf{B} \otimes \mathbf{C})$ and $[\mathbf{A}, \mathbf{B}] \otimes \mathbf{C} = [\mathbf{A} \otimes \mathbf{C}, \mathbf{B} \otimes \mathbf{C}]$, and noting that both matrices $\mathbf{W}_{l-1}^{(a)}$ and $\mathbf{I}_{2^{l-1}}$ have 2^{l-1} columns and the operator $\mathbf{P}_{\mathcal{T}_l}^\top$ selects only the columns indexed in $\mathcal{T}_l = \{2^{l-1} + 1, \dots, 2^l\}$, we get

$$\mathbf{W}_r^{(a)} \mathbf{P}_{\mathcal{T}_l}^\top = 2^{\frac{l-r-1}{2}} \left[\mathbf{W}_{l-1}^{(a)} \otimes \mathbf{1}_{2^{r-l+1}}, \mathbf{I}_{2^{l-1}} \otimes \begin{bmatrix} \mathbf{1}_{2^{r-l}} \\ (-1)^a \mathbf{1}_{2^{r-l}} \end{bmatrix}, \mathbf{0} \right] \mathbf{P}_{\mathcal{T}_l}^\top = 2^{\frac{l-r-1}{2}} \mathbf{I}_{2^{l-1}} \otimes \begin{bmatrix} \mathbf{1}_{2^{r-l}} \\ (-1)^a \mathbf{1}_{2^{r-l}} \end{bmatrix}. \quad (35)$$

By expanding the right-hand side of (35), the $(i, j)^{\text{th}}$ component of the matrix $\mathbf{W}_r^{(a)} \mathbf{P}_{\mathcal{T}_l}^\top$ reads

$$\left(\mathbf{W}_r^{(a)} \mathbf{P}_{\mathcal{T}_l}^\top \right)_{i,j} = \begin{cases} 2^{\frac{l-r-1}{2}}, & \text{if } (j-1)2^{r-l+1} + 1 \leq i < (j + \frac{1}{2})2^{r-l+1} + 1, \\ (-1)^a 2^{\frac{l-r-1}{2}}, & \text{if } (j + \frac{1}{2})2^{r-l+1} + 1 \leq i < (j+1)2^{r-l+1} + 1, \\ 0, & \text{otherwise.} \end{cases} \quad (36)$$

By comparing (36) with (16) and (18), we conclude that $(\Psi_l^{(a)})_{i,j} = (\mathbf{W}_r \mathbf{P}_{\mathcal{T}_l}^\top)_{i,j} = h_{l-1, j-1}^{(a)}(i-1)$, which completes the proof.

Lemma 5. For $a \in \{0, 1\}$ and $q_l = 2^{r-1} \cdot \sum_{k=0}^{r-l} 2^{-k}$,

$$\mathbf{W}_r^{(a)} \bar{\mathbf{P}}_{\mathcal{T}_{<l}}^\top = 2^{\frac{l-r-1}{2}} \left[\mathbf{W}_{l-1}^{(a)} \otimes \mathbf{1}_{2^{r-l+1}}, \mathbf{0}_{2^r \times q_l} \right].$$

Proof. We prove this lemma by induction over the value of l . From (17) or (19) and the definition of $\bar{\mathbf{P}}_{\mathcal{T}_{<r}}^\top$ one can observe that the base case $\mathbf{W}_r^{(a)} \bar{\mathbf{P}}_{\mathcal{T}_{<r}}^\top = 2^{\frac{-1}{2}} \left[\mathbf{W}_{r-1}^{(a)} \otimes \mathbf{1}_2, \mathbf{0}_{2^r \times 2^{r-1}} \right]$ is true. We now show that if the statement of the lemma holds for $l = j+1$ (induction hypothesis), then it holds for $l = j$. Since $\mathcal{T}_{<j} \subset \mathcal{T}_{<j+1}$, we have $\bar{\mathbf{P}}_{\mathcal{T}_{<j}} \bar{\mathbf{P}}_{\mathcal{T}_{<j+1}} = \bar{\mathbf{P}}_{\mathcal{T}_{<j}}$, and using the induction hypothesis we can write

$$\mathbf{W}_r^{(a)} \bar{\mathbf{P}}_{\mathcal{T}_{<j}}^\top = \mathbf{W}_r^{(a)} \bar{\mathbf{P}}_{\mathcal{T}_{<j+1}}^\top \bar{\mathbf{P}}_{\mathcal{T}_{<j}}^\top = 2^{\frac{j-r}{2}} \left[\mathbf{W}_j^{(a)} \otimes \mathbf{1}_{2^{r-j}}, \mathbf{0}_{2^r \times q_{j+1}} \right] \bar{\mathbf{P}}_{\mathcal{T}_{<j}}^\top. \quad (37)$$

By injecting the recursion formula of $\mathbf{W}_r^{(0)}$ and $\mathbf{W}_r^{(1)}$ from (17) and (19) (with $r = j$) in (37), $(\mathbf{A} \otimes \mathbf{B}) \otimes \mathbf{C} = \mathbf{A} \otimes (\mathbf{B} \otimes \mathbf{C})$ and $[\mathbf{A}, \mathbf{B}] \otimes \mathbf{C} = [\mathbf{A} \otimes \mathbf{C}, \mathbf{B} \otimes \mathbf{C}]$, we get

$$\mathbf{W}_r^{(a)} \bar{\mathbf{P}}_{\mathcal{T}_{<j}}^\top = 2^{\frac{j-r-1}{2}} \left[\mathbf{W}_{j-1}^{(a)} \otimes \mathbf{1}_{2^{r-j+1}}, \mathbf{0}_{2^r \times 2^{j-1}}, \mathbf{0}_{2^r \times q_{j+1}} \right], \quad (38)$$

since $\mathcal{T}_{<j} = \llbracket 2^{j-1} \rrbracket$ and $\bar{\mathbf{P}}_{\mathcal{T}_{<j}}^\top$ preserves the first 2^{j-1} columns of $\mathbf{W}_r^{(a)}$. Noting that $q_{j+1} + 2^{j-1} = q_j$ confirms the statement of the lemma for $n = j$ and thus, completes the proof. \square

5.2 Proof of Prop. 1

From the definitions of the Hadamard and DHW bases in Sec. 3.1, we quickly obtain $U_0^{(1)} = H_0^\top W_0^{(1)} = [1]$ and $U_0^{(0)} = H_0^\top W_0^{(0)} = [1]$. Since $(A \otimes B)(C \otimes D) = (AC) \otimes (BD)$, we get, for $r \geq 1$,

$$\begin{aligned} H_r^\top W_r^{(1)} &= \frac{1}{2} \begin{bmatrix} (H_{r-1}^\top \otimes [1 \ 1]) (W_{r-1}^{(1)} \otimes [\frac{1}{1}]) & (H_{r-1}^\top \otimes [1 \ 1]) (I_{2^{r-1}} \otimes [\frac{-1}{1}]) \\ (H_{r-1}^\top \otimes [1 \ -1]) (W_{r-1}^{(1)} \otimes [\frac{1}{1}]) & (H_{r-1}^\top \otimes [1 \ -1]) (I_{2^{r-1}} \otimes [\frac{-1}{1}]) \end{bmatrix} \\ &= \frac{1}{2} \begin{bmatrix} H_{r-1}^\top W_{r-1}^{(1)} \otimes [2] & H_{r-1}^\top I_{2^{r-1}} \otimes [0] \\ H_{r-1}^\top W_{r-1}^{(1)} \otimes [0] & H_{r-1}^\top I_{2^{r-1}} \otimes [2] \end{bmatrix} = \begin{bmatrix} H_{r-1} W_{r-1}^{(1)} & \mathbf{0} \\ \mathbf{0} & H_{r-1} \end{bmatrix}. \end{aligned}$$

Similarly, we can write

$$\begin{aligned} H_r^\top W_r^{(0)} &= \frac{1}{2} \begin{bmatrix} (H_{r-1}^\top \otimes [1 \ 1]) (W_{r-1}^{(0)} \otimes [\frac{1}{1}]) & (H_{r-1}^\top \otimes [1 \ 1]) (I_{2^{r-1}} \otimes [\frac{1}{1}]) \\ (H_{r-1}^\top \otimes [1 \ -1]) (W_{r-1}^{(0)} \otimes [\frac{1}{1}]) & (H_{r-1}^\top \otimes [1 \ -1]) (I_{2^{r-1}} \otimes [\frac{1}{1}]) \end{bmatrix} \\ &= \frac{1}{2} \begin{bmatrix} H_{r-1}^\top W_{r-1}^{(0)} \otimes [2] & H_{r-1}^\top I_{2^{r-1}} \otimes [2] \\ H_{r-1}^\top W_{r-1}^{(0)} \otimes [0] & H_{r-1}^\top I_{2^{r-1}} \otimes [0] \end{bmatrix}. \end{aligned}$$

By recursion, and from the definition of the 1-D dyadic levels \mathcal{T}^{1d} we then get the structure described in Fig. 2. Moreover, from Fig. 2-left and using the fact that H_r is symmetric, we conclude that $U_r^{(1)}$ is symmetric as well.

5.3 Proof of Prop. 2

From Remark 1 and Remark 2 we can write, for $t \xleftrightarrow{r+1} (t_1 + 1, t_2 + 1)$ and $l \xleftrightarrow{r+1} (l_1 + 1, l_2 + 1)$,

$$P_{\mathcal{T}_t^{\text{aniso}}} \Phi_{2\text{had}}^\top \Psi_{\text{adhw}} P_{\mathcal{T}_l^{\text{aniso}}}^\top = (P_{\mathcal{T}_{t_2}^{1d}} H_{t_2} W_{l_2}^{(1)} P_{\mathcal{T}_{l_2}^{1d}}^\top) \otimes (P_{\mathcal{T}_{t_1}^{1d}} H_{t_1} W_{l_1}^{(1)} P_{\mathcal{T}_{l_1}^{1d}}^\top) \in \mathbb{R}^{2^{t_1+t_2-2} \times 2^{l_1+l_2-2}},$$

and this matrix, using (26a), is $H_{(t_2-1)_+} \otimes H_{(t_1-1)_+}$, if $t_1 = l_1$ and $t_2 = l_2$ (and $\mathbf{0}$ otherwise).

We now prove the second part of the proposition, and we simply write \mathcal{T}_l for \mathcal{T}_l^{1d} . Recall from the definition of the IDHW basis and the 2-D isotropic wavelet levels in Sec. 3.1 that

$$\Psi_{\text{idhw}} P_{\mathcal{T}_l^{\text{iso}}}^\top = \left[(W_r^{(0)} P_{\mathcal{T}_l}^\top) \otimes (W_r^{(1)} P_{\mathcal{T}_l}^\top), (W_r^{(1)} P_{\mathcal{T}_l}^\top) \otimes (W_r^{(1)} P_{\mathcal{T}_l}^\top), (W_r^{(1)} P_{\mathcal{T}_l}^\top) \otimes (W_r^{(0)} P_{\mathcal{T}_l}^\top) \right], \quad (39)$$

for $l \in \llbracket r \rrbracket$. Define $U^{(1)} := H_r W_r^{(1)}$ and $U^{(0)} := H_r W_r^{(0)}$, and $V^{(t,l)} := P_{\mathcal{T}_t^{\text{iso}}} \Phi_{2\text{had}}^\top \Psi_{\text{idhw}} P_{\mathcal{T}_l^{\text{iso}}}^\top$.

For the proof we need to compute $V^{(t,l)}$ for $t, l \in \llbracket r \rrbracket_0$. First, we assume that $t, l \in \llbracket r \rrbracket$. From Remark 2 and (39) we have

$$V^{(t,l)} = \begin{bmatrix} (P_{\mathcal{T}_{<t}} U^{(0)} P_{\mathcal{T}_l}^\top) \otimes (P_{\mathcal{T}_t} U^{(1)} P_{\mathcal{T}_l}^\top) & (P_{\mathcal{T}_{<t}} U^{(1)} P_{\mathcal{T}_l}^\top) \otimes (P_{\mathcal{T}_t} U^{(1)} P_{\mathcal{T}_l}^\top) & (P_{\mathcal{T}_{<t}} U^{(1)} P_{\mathcal{T}_l}^\top) \otimes (P_{\mathcal{T}_t} U^{(0)} P_{\mathcal{T}_l}^\top) \\ (P_{\mathcal{T}_t} U^{(0)} P_{\mathcal{T}_l}^\top) \otimes (P_{\mathcal{T}_t} U^{(1)} P_{\mathcal{T}_l}^\top) & (P_{\mathcal{T}_t} U^{(1)} P_{\mathcal{T}_l}^\top) \otimes (P_{\mathcal{T}_t} U^{(1)} P_{\mathcal{T}_l}^\top) & (P_{\mathcal{T}_t} U^{(1)} P_{\mathcal{T}_l}^\top) \otimes (P_{\mathcal{T}_t} U^{(0)} P_{\mathcal{T}_l}^\top) \\ (P_{\mathcal{T}_t} U^{(0)} P_{\mathcal{T}_l}^\top) \otimes (P_{\mathcal{T}_{<t}} U^{(1)} P_{\mathcal{T}_l}^\top) & (P_{\mathcal{T}_t} U^{(1)} P_{\mathcal{T}_l}^\top) \otimes (P_{\mathcal{T}_{<t}} U^{(1)} P_{\mathcal{T}_l}^\top) & (P_{\mathcal{T}_t} U^{(1)} P_{\mathcal{T}_l}^\top) \otimes (P_{\mathcal{T}_{<t}} U^{(0)} P_{\mathcal{T}_l}^\top) \end{bmatrix}.$$

From Remark 3 (with an attention to the conditions on the right-hand side of the relations) we observe that the diagonal blocks in $V^{(t,l)}$ are equal to $H_{t-1} \otimes H_{t-1}$ if $t = l$ and $\mathbf{0}$ otherwise. Therefore, if $t = l$,

$$V^{(t,l)} = \begin{bmatrix} H_{(t-1)} \otimes H_{(t-1)} & \mathbf{0} & \mathbf{0} \\ \mathbf{0} & H_{(t-1)} \otimes H_{(t-1)} & \mathbf{0} \\ \mathbf{0} & \mathbf{0} & H_{(t-1)} \otimes H_{(t-1)} \end{bmatrix} = I_3 \otimes (H_{(t-1)} \otimes H_{(t-1)}),$$

while $\mathbf{V}^{(t,l)} = \mathbf{0}$ if $t \neq l$. Second, we compute $\mathbf{V}^{(t,l)}$ for $t \in \llbracket r \rrbracket_0$ and $l = 0$. Since $\Psi_{\text{idhw}} \mathbf{P}_{\mathcal{T}_0^{\text{iso}}}^\top = (\mathbf{W}_r^{(0)} \mathbf{P}_{\mathcal{T}_0}^\top) \otimes (\mathbf{W}_r^{(0)} \mathbf{P}_{\mathcal{T}_0}^\top)$, $\mathbf{U}^{(0)} \mathbf{P}_{\mathcal{T}_0}^\top = \mathbf{I}_{2^r} \mathbf{P}_{\{1\}}^\top$, and from Remark 2, we have

$$\mathbf{V}^{(t,0)} = \begin{bmatrix} (\mathbf{P}_{\mathcal{T}_{<t}} \mathbf{U}^{(0)} \mathbf{P}_{\mathcal{T}_0}^\top) \otimes (\mathbf{P}_{\mathcal{T}_t} \mathbf{U}^{(0)} \mathbf{P}_{\mathcal{T}_0}^\top) \\ (\mathbf{P}_{\mathcal{T}_t} \mathbf{U}^{(0)} \mathbf{P}_{\mathcal{T}_0}^\top) \otimes (\mathbf{P}_{\mathcal{T}_t} \mathbf{U}^{(0)} \mathbf{P}_{\mathcal{T}_0}^\top) \\ (\mathbf{P}_{\mathcal{T}_t} \mathbf{U}^{(0)} \mathbf{P}_{\mathcal{T}_0}^\top) \otimes (\mathbf{P}_{\mathcal{T}_{<t}} \mathbf{U}^{(0)} \mathbf{P}_{\mathcal{T}_0}^\top) \end{bmatrix} = \begin{bmatrix} \mathbf{P}_{\overline{\mathcal{T}_t \times \mathcal{T}_{<t}}} \mathbf{I}_{2^{2r}} \mathbf{P}_{\{1\}}^\top \\ \mathbf{P}_{\overline{\mathcal{T}_t \times \mathcal{T}_t}} \mathbf{I}_{2^{2r}} \mathbf{P}_{\{1\}}^\top \\ \mathbf{P}_{\overline{\mathcal{T}_{<t} \times \mathcal{T}_t}} \mathbf{I}_{2^{2r}} \mathbf{P}_{\{1\}}^\top \end{bmatrix} = \mathbf{P}_{\mathcal{T}_t^{\text{iso}}} [1, \mathbf{0}]^\top.$$

Finally, we need to compute $\mathbf{V}^{(t,l)}$ for $t = 0$ and $l \in \llbracket r \rrbracket$, *i.e.*,

$$\mathbf{V}^{(0,l)} = [(\mathbf{P}_{\mathcal{T}_0} \mathbf{U}^{(0)} \mathbf{P}_{\mathcal{T}_l}^\top) \otimes (\mathbf{P}_{\mathcal{T}_0} \mathbf{U}^{(1)} \mathbf{P}_{\mathcal{T}_l}^\top) \quad (\mathbf{P}_{\mathcal{T}_0} \mathbf{U}^{(1)} \mathbf{P}_{\mathcal{T}_l}^\top) \otimes (\mathbf{P}_{\mathcal{T}_0} \mathbf{U}^{(1)} \mathbf{P}_{\mathcal{T}_l}^\top) \quad (\mathbf{P}_{\mathcal{T}_0} \mathbf{U}^{(1)} \mathbf{P}_{\mathcal{T}_l}^\top) \otimes (\mathbf{P}_{\mathcal{T}_0} \mathbf{U}^{(0)} \mathbf{P}_{\mathcal{T}_l}^\top)].$$

Using (26a) and (26c) with $t = 0$ and $l \in \llbracket r \rrbracket$ yields $\mathbf{V}^{(0,l)} = \mathbf{0}$. This completes the proof.

5.4 Proof of Prop. 3

In this proof we write \mathcal{T}_l for \mathcal{T}_l^{1d} . Recall that $\mu(\mathbf{H}_r) = 2^{-r/2}$, and for any $k > 1$, $k \in \mathcal{T}_{\bar{l}(k)}$ with $\bar{l}(k) := \lfloor \log_2(k-1) \rfloor + 1$, since $\mathcal{T}_l = \llbracket 2^l \rrbracket \setminus \llbracket 2^{l-1} \rrbracket$, for $l \geq 1$. We first observe that $\mu_1^{\text{loc}}(\mathbf{U}_r^{(1)}) = 1$, since $(\mathbf{H}_r)_{1,i} = (\mathbf{W}_r^{(1)})_{1,i} = 2^{-r/2}$ for all $i \in \llbracket 2^r \rrbracket$.

To prove (28a), note that, for $k > 1$, since $\bar{\mathbf{P}}_\Omega = \mathbf{P}_\Omega^\top \mathbf{P}_\Omega$, for any subset Ω , and $\mathbf{P}_{\{k\}} \bar{\mathbf{P}}_{\mathcal{T}_{\bar{l}(k)}} = \mathbf{P}_{\{k\}}$, $|(\mathbf{H}_r)_{i,j}| = 2^{-r/2}$ for all $i, j \in \llbracket 2^r \rrbracket$ and using (26a),

$$\mu_k^{\text{loc}}(\mathbf{U}_{2^r}^{(1)}) = \mu(\mathbf{P}_{\{k\}} \bar{\mathbf{P}}_{\mathcal{T}_{\bar{l}(k)}} \mathbf{U}_{2^r}^{(1)}) = \mu(\mathbf{P}_{\{k\}} \mathbf{H}_{\bar{l}(k)-1}) = 2^{-\frac{\bar{l}(k)-1}{2}} = 2^{-\frac{\lfloor \log_2(k-1) \rfloor}{2}}.$$

In addition, $\|\boldsymbol{\mu}^{\text{loc}}(\mathbf{U}_r^{(1)})\|_2^2 = 1 + \sum_{k=2}^N 2^{-\lfloor \log_2(k-1) \rfloor} = 1 + \sum_{l=0}^{r-1} 2^l \cdot 2^{-l} = \log_2(N) + 1$.

Next, to prove (28b), we first note that $\mu_1^{\text{loc}}(\Phi_{2\text{had}}^\top \Psi_{\text{idhw}}) = 1$, since $(\Phi_{2\text{had}})_{1,i} = (\Psi_{\text{idhw}})_{1,i} = 2^{-r}$ for all $i \in \llbracket 2^{2r} \rrbracket$. Consider the rule $k \xrightarrow{N} (k_1, k_2)$. Using (27b) and (33b), for $1 < k \in \mathcal{T}_t^{\text{iso}}$,

$$\mu_k^{\text{loc}}(\Phi_{2\text{had}}^\top \Psi_{\text{idhw}}) = \mu_{k_1}^{\text{loc}}(\mathbf{H}_{(t-1)}) \cdot \mu_{k_2}^{\text{loc}}(\mathbf{H}_{(t-1)}) = 2^{-(t-1)}. \quad (40)$$

Moreover, we find

$$k \in \mathcal{T}_t^{\text{iso}} \quad \Leftrightarrow \quad \max(k_1, k_2) \in \mathcal{T}_t \quad \Leftrightarrow \quad t-1 = \lfloor \log_2(\max(k_1, k_2) - 1) \rfloor. \quad (41)$$

Combining (40) and (41) implies the local coherence relation in (28b).

Moreover, since $|\mathcal{T}_t^{\text{iso}}| = 3 \cdot 2^{2(t-1)}$ for $t \in \llbracket r \rrbracket$, (40) provides

$$\|\boldsymbol{\mu}^{\text{loc}}(\Phi_{2\text{had}}^\top \Psi_{\text{idhw}})\|_2^2 = 1 + \sum_{t=1}^r \sum_{k \in \mathcal{T}_t^{\text{iso}}} \mu_k^{\text{loc}}(\Phi_{2\text{had}}^\top \Psi_{\text{idhw}})^2 = 1 + \sum_{t=1}^r |\mathcal{T}_t^{\text{iso}}| \cdot 2^{-2(t-1)} = 1 + 3 \cdot r.$$

Finally, to prove (28c), we first observe that $\mu_1^{\text{loc}}(\Phi_{2\text{had}}^\top \Psi_{\text{adhw}}) = 1$, since $(\Phi_{2\text{had}})_{1,i} = (\Psi_{\text{adhw}})_{1,i} = 2^{-r}$ for all $i \in \llbracket 2^{2r} \rrbracket$. Consider the rules $t \xrightarrow{r+1} (t_1+1, t_2+1)$ and $k \xrightarrow{N} (k_1, k_2)$. From the construction of the 2-D anisotropic levels we have, for $k > 1$,

$$k \in \mathcal{T}_t^{\text{aniso}} \quad \Leftrightarrow \quad k_1 \in \mathcal{T}_{t_1}, k_2 \in \mathcal{T}_{t_2} \quad \Leftrightarrow \quad t_1 - 1 = \lfloor \log_2(k_1 - 1) \rfloor, t_2 - 1 = \lfloor \log_2(k_2 - 1) \rfloor. \quad (42)$$

Using (27a) and (33b), for $1 < k \in \mathcal{T}_t^{\text{aniso}}$, we get

$$\mu_k^{\text{loc}}(\Phi_{2\text{had}}^\top \Psi_{\text{adhw}}) = \mu_k^{\text{loc}}(\mathbf{H}_{t_2-1} \otimes \mathbf{H}_{t_1-1}) = \mu_{k_1}^{\text{loc}}(\mathbf{H}_{t_1-1}) \cdot \mu_{k_2}^{\text{loc}}(\mathbf{H}_{t_2-1}). \quad (43)$$

Combining (42) and (43) with the relation in 28a implies the local coherence value in (28c).

In addition, using (28a),

$$\|\boldsymbol{\mu}^{\text{loc}}(\Phi_{2\text{had}}^\top \Psi_{\text{adhw}})\|_2^2 = \left(1 + \sum_{k_1=2}^N 2^{-\lfloor \log_2(k_1-1) \rfloor}\right) \cdot \left(1 + \sum_{k_2=2}^N 2^{-\lfloor \log_2(k_2-1) \rfloor}\right) = (\log_2(N) + 1)^2.$$

5.5 Proof of Prop. 4

Given $\mathbf{U}_r^{(1)} = \mathbf{H}_r \mathbf{W}_r^{(1)}$, and $\mathcal{T}_l = \mathcal{T}_l^{\text{1d}}$ for $l \in \llbracket r \rrbracket_0$, we note that $\mu(\mathbf{H}_r) = 2^{-r/2}$, $\mu(\mathbf{P}_{\mathcal{W}_t} \mathbf{A}) = \max_l \mu(\mathbf{P}_{\mathcal{W}_t} \mathbf{A} \mathbf{P}_{\mathcal{S}_l}^\top)$, and for any orthonormal matrix Φ , $\|\Phi\|_{2,2} = \max_{\|\mathbf{v}\|_2=1} \|\Phi \mathbf{v}\|_2 = \|\mathbf{v}\|_2 = 1$.

We first prove (30a). From Remark 3, note that $\mu(\mathbf{P}_{\mathcal{T}_t} \mathbf{U}_r^{(1)} \mathbf{P}_{\mathcal{T}_0}^\top) = \delta_{t,0}$ and for $l \in \llbracket r \rrbracket$,

$$\mu(\mathbf{P}_{\mathcal{T}_t} \mathbf{U}_r^{(1)} \mathbf{P}_{\mathcal{T}_l}^\top) = \mu(\mathbf{H}_{t-1}) \cdot \delta_{t,l} = 2^{-(t-1)/2} \cdot \delta_{t,l}. \quad (44)$$

Therefore, for $t, l \in \llbracket r \rrbracket_0$ we obtain $\mu(\mathbf{P}_{\mathcal{T}_t} \mathbf{U}_r^{(1)}) = 2^{-\frac{(t-1)_+}{2}}$, $\mu_{t,l}^{\mathcal{T},\mathcal{T}}(\mathbf{U}^{(1)}) = 2^{-(t-1)_+} \cdot \delta_{t,l}$. To compute the relative sparsity, from Lemma 1 and Remark 3, and since $\|\mathbf{H}_r\|_{2,2} = 1$, we find

$$K_t^{\mathcal{T},\mathcal{T}}(\mathbf{U}^{(1)}, \mathbf{k})^{1/2} \leq \sum_{l=0}^r \|\mathbf{P}_{\mathcal{T}_t} \mathbf{U}^{(1)} \mathbf{P}_{\mathcal{T}_l}^\top\|_{2,2} \sqrt{k_l} = \|\mathbf{H}_{(t-1)_+}\|_{2,2} \sqrt{k_t} = \sqrt{k_t}. \quad (45)$$

To prove (30b), note from (27b) that $\mu(\mathbf{P}_{\mathcal{T}_t^{\text{iso}}} \Phi_{2\text{had}}^\top \Psi_{\text{idhw}} \mathbf{P}_{\mathcal{T}_0^{\text{iso}}}^\top) = \delta_{t,0}$, and, for $l \in \llbracket r \rrbracket$,

$$\mu(\mathbf{P}_{\mathcal{T}_t^{\text{iso}}} \Phi_{2\text{had}}^\top \Psi_{\text{idhw}} \mathbf{P}_{\mathcal{T}_l^{\text{iso}}}^\top) = \mu(\mathbf{I}_3) \cdot \mu(\mathbf{H}_{(t-1)}) \cdot \mu(\mathbf{H}_{(l-1)}) \cdot \delta_{t,l} = 2^{-(t-1)} \cdot \delta_{t,l}, \quad (46)$$

where we used the rule in (33a). Therefore, for $t, l \in \llbracket r \rrbracket_0$ we obtain $\mu(\mathbf{P}_{\mathcal{T}_t^{\text{iso}}} \Phi_{2\text{had}}^\top)$ and $\mu_{t,l}^{\mathcal{T}^{\text{iso}},\mathcal{T}^{\text{iso}}}(\Phi_{2\text{had}}^\top \Psi_{\text{idhw}}) = 2^{-2(t-1)_+} \cdot \delta_{t,l}$. To compute the relative sparsity, from Lemma 1 and Prop. 2, we have

$$K_t^{\mathcal{T}^{\text{iso}},\mathcal{T}^{\text{iso}}}(\Phi_{2\text{had}}^\top \Psi_{\text{idhw}}, \mathbf{k})^{1/2} \leq \sqrt{k_0} \cdot \delta_{t,0} + \sum_{l=1}^r \|\mathbf{I}_3 \otimes (\mathbf{H}_{(l-1)} \otimes \mathbf{H}_{(l-1)})\|_{2,2} \sqrt{k_l} \cdot \delta_{t,l} = \sqrt{k_t}. \quad (47)$$

We now prove (30c). Consider $t, l \in \llbracket (r+1)^2 \rrbracket$ such that $t \xrightarrow{r+1} (t_1+1, t_2+1)$, $l \xrightarrow{r+1} (l_1+1, l_2+1)$ and $t_1, t_2, l_1, l_2 \in \llbracket r \rrbracket_0$. From (27a) and using (33a) we have

$$\mu(\mathbf{P}_{\mathcal{T}_t^{\text{aniso}}} \Phi_{2\text{had}}^\top \Psi_{\text{adhw}} \mathbf{P}_{\mathcal{T}_l^{\text{aniso}}}^\top) = \mu(\mathbf{H}_{(t_1-1)_+}) \cdot \mu(\mathbf{H}_{(t_2-1)_+}) \cdot \delta_{t_1,l_1} \cdot \delta_{t_2,l_2} = 2^{-\frac{(t_1-1)_+}{2}} \cdot 2^{-\frac{(t_2-1)_+}{2}} \cdot \delta_{t_1,l_1} \cdot \delta_{t_2,l_2}. \quad (48)$$

Therefore, $\mu(\mathbf{P}_{\mathcal{T}_t^{\text{aniso}}} \Phi_{2\text{had}}^\top) = 2^{-\frac{(t_1-1)_+}{2}} \cdot 2^{-\frac{(t_2-1)_+}{2}}$, $\mu_{t,l}^{\mathcal{T}^{\text{aniso}},\mathcal{T}^{\text{aniso}}}(\Phi_{2\text{had}}^\top \Psi_{\text{adhw}}) = 2^{-(t_1-1)_+} \cdot 2^{-(t_2-1)_+} \cdot \delta_{t_1,l_1} \cdot \delta_{t_2,l_2}$. To compute the relative sparsity, from Lemma 1 and Prop. 2, we have

$$K_t^{\mathcal{T}^{\text{aniso}},\mathcal{T}^{\text{aniso}}}(\Phi_{2\text{had}}^\top \Psi_{\text{adhw}}, \mathbf{k})^{1/2} \leq \sum_{l=1}^{(r+1)^2} \|\mathbf{H}_{(l_2-1)_+} \otimes \mathbf{H}_{(l_1-1)_+}\|_{2,2} \sqrt{k_l} \cdot \delta_{t,l} = \sqrt{k_t}. \quad (49)$$

5.6 Proof of Thm. 4

Following Thm. 2, since in all cases covered by Thm. 4 (*i.e.*, 1-D Hadamard-Haar, 2-D isotropic Hadamard-Haar, and 2-D anisotropic Hadamard-Haar) we have $\mathcal{W} = \mathcal{S}$, we need to show that the sample-complexity bound for each case satisfies

$$\begin{aligned} m_t &\gtrsim |\mathcal{S}_t| \cdot \left(\sum_{l=1}^{|\mathcal{S}|} \mu_{t,l}^{\mathcal{S},\mathcal{S}}(\Phi^\top \Psi) \cdot k_l \right) \cdot \log(K\epsilon^{-1}) \cdot \log(N), \\ m_t &\gtrsim \hat{m}_t \cdot \log(K\epsilon^{-1}) \cdot \log(N), \end{aligned}$$

where \hat{m}_t must satisfy

$$\sum_{t=1}^{|\mathcal{S}|} \frac{|\mathcal{S}_t| \cdot \mu_{t,l}^{\mathcal{S},\mathcal{S}}(\Phi^\top \Psi) \cdot K_t^{\mathcal{S},\mathcal{S}}(\Phi^\top \Psi, \mathbf{k})}{\hat{m}_t} \lesssim 1, \quad \text{for } l \in \llbracket |\mathcal{S}| \rrbracket.$$

Moreover, since in the three covered cases the multilevel coherence $\mu_{t,l}^{\mathcal{S},\mathcal{S}}(\Phi^\top \Psi)$ vanishes for $t \neq l$, and $\mu_{t,l}^{\mathcal{S},\mathcal{S}}(\Phi^\top \Psi) = |\mathcal{S}_l|^{-1}$ for $t = l$, the proof is further simplified, as the condition on \hat{m}_t holds if $\hat{m}_l \gtrsim K_l^{\mathcal{S},\mathcal{S}}(\Phi^\top \Psi, \mathbf{k})$. Thus, it suffices to show that in each case

$$m_t \gtrsim \max \left(K_t^{\mathcal{S},\mathcal{S}}(\Phi^\top \Psi, \mathbf{k}), k_t \right) \cdot \log(K\epsilon^{-1}) \cdot \log(N).$$

However, for the three cases, $\max \left(K_t^{\mathcal{S},\mathcal{S}}(\Phi^\top \Psi, \mathbf{k}), k_t \right) = k_t$. Therefore, $m_t \gtrsim k_t \cdot \log(K\epsilon^{-1}) \cdot \log(N)$ for all the three cases, which completes the proof.

6 Discussion

This work has studied the Hadamard-Haar systems in the context of CS theory, *i.e.*, the problem of recovering signals from subsampled Hadamard measurements using Haar wavelet sparsity basis.

Traditional UDS scheme is inapplicable in Hadamard-Haar systems, since the Hadamard and Haar bases are maximally coherent. The new CS principles, *i.e.*, local and multilevel coherences, introduced by Krahmer and Ward [13] and by Adcock *et al.* [26], respectively, inspired us to design sampling strategies that require minimum number of Hadamard measurements and in the same time allow stable and robust signal recovery. By computing the exact values of local and multilevel coherences we achieved the tight sample-complexity bounds for both uniform and non-uniform recovery guarantees. In two-dimensions, we considered two constructions of the 2-D Haar wavelet basis, *i.e.*, using either tensor product of two 1-D Haar bases or the isotropic construction of a multi-resolution analysis; and observed that an efficient design of sampling strategy for each system is unique.

Our results have been illustrated by several numerical tests for different types of signals with varying resolution, sparsity, and number of measurements. In particular, we have numerically demonstrated the impact of the resolution in signal recovery.

Our uniform recovery guarantee in Thm. 3 is linked to the ℓ_1 minimization problem (8). A variant of this problem would be to replace the ℓ_1 -norm term with the total variation norm. Following the proof of Thm. 3.1 in [13] we believe that the same sample-complexity bounds and sampling

strategies as in Thm. 3 provides stable and robust signal recovery (from subsampled Hadamard measurements) via the total variation norm minimization problem. However, we postpone this potential extension to a future study.

As mentioned in the introduction, Li and Adcock [17] have recently developed a uniform version of the recovery guarantee for MDS scheme in Prop. 2. The computed multilevel coherences in Prop. 4 can be directly applied to the sample-complexity bound in [17, Thm. 3.1]. Due to the uniform recovery nature of Thm. 3.1 in [17], the final sample-complexity bounds for Hadamard-Haar systems, in the context of MDS scheme, would be the same as the ones in Thm. 4 up to some extra log factors.

Following the uncovered cells in Table. 1, a line of study would be to characterize the effect of the other sparsity bases on our local and multilevel coherence analysis, *e.g.*, the 2-D Daubechies wavelets.

Finally, in this respect, it is worth mentioning that the recurrence relations provided by the Kronecker factorization in (17) and (24) goes beyond the Hadamard and Haar matrices. In fact, the Kronecker product has been used to describe a range of other unitary matrices, *e.g.*, the discrete Fourier transform and the related Sine, Cosine, and Hartley transforms [78–80]; see also [81] for the factorization of the Daubechies wavelets. An interesting research would be to investigate the combinations of different sensing and sparsity bases and to find other scaling structures.

Acknowledgment

We would like to thank Ben Adcock for the his valuable remarks during the iTWIST’18 workshop (Marseille, France).

References

- [1] D. L. Donoho, “Compressed sensing,” *IEEE transactions on information theory*, vol. 52, no. 4, pp. 1289–1306, 2006.
- [2] E. J. Candès and T. Tao, “Near-optimal signal recovery from random projections: Universal encoding strategies?” *IEEE transactions on information theory*, vol. 52, no. 12, pp. 5406–5425, 2006.
- [3] M. Lustig, D. L. Donoho, J. M. Santos, and J. M. Pauly, “Compressed sensing MRI,” *IEEE signal processing magazine*, vol. 25, no. 2, pp. 72–82, 2008.
- [4] V. Studer, J. Bobin, M. Chahid, H. S. Mousavi, E. Candès, and M. Dahan, “Compressive fluorescence microscopy for biological and hyperspectral imaging,” *Proceedings of the National Academy of Sciences*, vol. 109, no. 26, pp. E1679–E1687, 2012.
- [5] B. Roman, A. C. Hansen, and B. Adcock, “On asymptotic structure in compressed sensing,” *arXiv preprint arXiv:1406.4178*, 2014.
- [6] M. F. Duarte, M. A. Davenport, D. Takhar, J. N. Laska, T. Sun, K. E. Kelly, and R. G. Baraniuk, “Single-pixel imaging via compressive sampling,” *IEEE signal processing magazine*, vol. 25, no. 2, p. 83, 2008.

- [7] E. Candès and J. Romberg, “Sparsity and incoherence in compressive sampling,” *Inverse problems*, vol. 23, no. 3, pp. 969–985, 2007.
- [8] B. Adcock, A. C. Hansen, and B. Roman, “The quest for optimal sampling: Computationally efficient, structure-exploiting measurements for compressed sensing,” in *Compressed Sensing and its Applications*. Springer, 2015, pp. 143–167.
- [9] L. Baldassarre, C. Aprile, M. Shoaran, Y. Leblebici, and V. Cevher, “Structured sampling and recovery of IEEG signals,” in *IEEE International Workshop on Computational Advances in Multi-Sensor Adaptive Processing*, no. EPFL-CONF-214740, 2015.
- [10] A. Moshtaghpour, J. M. Bioucas-Dias, and L. Jacques, “Compressive hyperspectral imaging: Fourier transform interferometry meets single pixel camera,” in *international Traveling Workshop on Interactions between low-complexity data models and Sensing Techniques (iTWIST)*, 2018.
- [11] —, “Compressive single-pixel Fourier transform imaging using structured illumination,” in *IEEE International Conference on Acoustics, Speech and Signal Processing (ICASSP)*, 2019, pp. 7810–7814.
- [12] B. Adcock, A. C. Hansen, C. Poon, and B. Roman, “Breaking the coherence barrier: A new theory for compressed sensing,” in *Forum of Mathematics, Sigma*, vol. 5. Cambridge University Press, 2017.
- [13] F. Krahmer and R. Ward, “Stable and robust sampling strategies for compressive imaging,” *IEEE transactions on image processing*, vol. 23, no. 2, pp. 612–622, 2014.
- [14] G. Puy, P. Vandergheynst, and Y. Wiaux, “On variable density compressive sampling,” *IEEE signal processing letters*, vol. 18, no. 10, pp. 595–598, 2011.
- [15] J. Bigot, C. Boyer, and P. Weiss, “An analysis of block sampling strategies in compressed sensing,” *IEEE transactions on information theory*, vol. 62, no. 4, pp. 2125–2139, 2016.
- [16] C. Boyer, J. Bigot, and P. Weiss, “Compressed sensing with structured sparsity and structured acquisition,” *Applied and Computational Harmonic Analysis*, 2017.
- [17] C. Li and B. Adcock, “Compressed sensing with local structure: uniform recovery guarantees for the sparsity in levels class,” *Applied and Computational Harmonic Analysis*, 2017.
- [18] S. Foucart and H. Rauhut, *A mathematical introduction to compressive sensing*. Birkhäuser Basel, 2013, vol. 1, no. 3.
- [19] E. J. Candès and T. Tao, “Decoding by linear programming,” *IEEE transactions on information theory*, vol. 51, no. 12, pp. 4203–4215, 2005.
- [20] Y. Tsaig and D. L. Donoho, “Extensions of compressed sensing,” *Signal processing*, vol. 86, no. 3, pp. 549–571, 2006.
- [21] Z. Wang and G. R. Arce, “Variable density compressed image sampling,” *IEEE transactions on image processing*, vol. 19, no. 1, pp. 264–270, 2010.

- [22] A. C. Polak, M. F. Duarte, and D. L. Goeckel, “Performance bounds for grouped incoherent measurements in compressive sensing,” *IEEE transactions on signal processing*, vol. 63, no. 11, pp. 2877–2887, 2015.
- [23] B. Adcock, C. Boyer, and S. Brugiapaglia, “On oracle-type local recovery guarantees in compressed sensing,” *arXiv preprint arXiv:1806.03789*, 2018.
- [24] H. Rauhut, “Compressive sensing and structured random matrices,” *Theoretical foundations and numerical methods for sparse recovery*, vol. 9, pp. 1–92, 2010.
- [25] B. Adcock, V. Antun, and A. C. Hansen, “Uniform recovery in infinite-dimensional compressed sensing and applications to structured binary sampling,” *arXiv preprint arXiv:1905.00126*, 2019.
- [26] B. Adcock, A. C. Hansen, and B. Roman, “A note on compressed sensing of structured sparse wavelet coefficients from subsampled Fourier measurements,” *IEEE signal processing letters*, vol. 23, no. 5, pp. 732–736, 2016.
- [27] M. Lustig, D. Donoho, and J. M. Pauly, “Sparse MRI: The application of compressed sensing for rapid MR imaging,” *Magnetic Resonance in Medicine: An Official Journal of the International Society for Magnetic Resonance in Medicine*, vol. 58, no. 6, pp. 1182–1195, 2007.
- [28] A. Moshtaghpour, V. Cambareri, K. Degraux, A. C. Gonzalez Gonzalez, M. Roblin, L. Jacques, and P. Antoine, “Coded-illumination Fourier transform interferometry,” in *the Golden Jubilee Meeting of the Royal Belgian Society for Microscopy (RBSM)*, 2016, pp. 65–66.
- [29] A. Moshtaghpour and L. Jacques, “Multilevel illumination coding for Fourier transform interferometry in fluorescence spectroscopy,” in *IEEE International Conference on Image Processing (ICIP)*, 2018, pp. 1433–1437.
- [30] A. Moshtaghpour, L. Jacques, V. Cambareri, P. Antoine, and M. Roblin, “A variable density sampling scheme for compressive Fourier transform interferometry,” *SIAM journal on imaging sciences*, vol. 12, no. 2, pp. 671–715, 2019.
- [31] A. Moshtaghpour, V. Cambareri, L. Jacques, P. Antoine, and M. Roblin, “Compressive hyperspectral imaging using coded Fourier transform interferometry,” in *Signal Processing with Adaptive Sparse Structured Representations workshop (SPARS)*, 2017.
- [32] A. Moshtaghpour, K. Degraux, V. Cambareri, A. Gonzalez, M. Roblin, L. Jacques, and P. Antoine, “Compressive hyperspectral imaging with Fourier transform interferometry,” in *3rd International Traveling Workshop on Interactions between Sparse models and Technology*, 2016, pp. 27–29.
- [33] G. Davis, M. Maggioni, F. Warner, and F. Geshwind, “Hyperspectral analysis of normal and malignant colon tissue microarray sections using a novel DMD system,” in *NIH Optical Imaging Workshop*, 2004.
- [34] G. Huang, H. Jiang, K. Matthews, and P. Wilford, “Lensless imaging by compressive sensing,” in *IEEE International Conference on Image Processing (ICIP)*, 2013, pp. 2101–2105.

- [35] Y. Zhang, M. P. Edgar, B. Sun, N. Radwell, G. M. Gibson, and M. J. Padgett, “3d single-pixel video,” *Journal of Optics*, vol. 18, no. 3, p. 035203, 2016.
- [36] T. Sun, G. Woods, M. F. Duarte, K. Kelly, C. Li, and Y. Zhang, “Obic measurements without lasers or raster-scanning based on compressive sensing,” in *International Symposium for Testing and Failure Analysis (ISTFA)*, San Jose, CA, 2009, pp. 272–277.
- [37] P. Clemente, V. Durán, E. Tajahuerce, P. Andrés, V. Climent, and J. Lancis, “Compressive holography with a single-pixel detector,” *Optics letters*, vol. 38, no. 14, pp. 2524–2527, 2013.
- [38] S. Jin, W. Hui, Y. Wang, K. Huang, Q. Shi, C. Ying, D. Liu, Q. Ye, W. Zhou, and J. Tian, “Hyperspectral imaging using the single-pixel Fourier transform technique,” *Scientific reports*, vol. 7, p. 45209, 2017.
- [39] L. Martínez-León, P. Clemente, Y. Mori, V. Climent, J. Lancis, and E. Tajahuerce, “Single-pixel digital holography with phase-encoded illumination,” *Optics express*, vol. 25, no. 5, pp. 4975–4984, 2017.
- [40] Z. Zhang, X. Wang, G. Zheng, and J. Zhong, “Hadamard single-pixel imaging versus Fourier single-pixel imaging,” *Optics Express*, vol. 25, no. 16, pp. 19 619–19 639, 2017.
- [41] R. DeVerse, F. Geshwind, R. Coifman, W. Fateley, and A. Coppi, “Application of spatial light modulators for new modalities in spectrometry and imaging,” Nov. 4 2004, US Patent App. 10/764,113.
- [42] M. Wakin, J. N. Laska, M. F. Duarte, D. Baron, S. Sarvotham, D. Takhar, K. F. Kelly, and R. G. Baraniuk, “Compressive imaging for video representation and coding,” in *Picture Coding Symposium*, vol. 1, 2006, p. 13.
- [43] B. Sun, M. P. Edgar, R. Bowman, L. E. Vittert, S. Welsh, A. Bowman, and M. Padgett, “3d computational imaging with single-pixel detectors,” *Science*, vol. 340, no. 6134, pp. 844–847, 2013.
- [44] J. Ma, “Single-pixel remote sensing,” *IEEE Geoscience and Remote Sensing Letters*, vol. 6, no. 2, pp. 199–203, 2009.
- [45] W. L. Chan, K. Charan, D. Takhar, K. F. Kelly, R. G. Baraniuk, and D. M. Mittleman, “A single-pixel terahertz imaging system based on compressed sensing,” *Applied Physics Letters*, vol. 93, no. 12, p. 121105, 2008.
- [46] D. Takhar, J. N. Laska, M. B. Wakin, M. F. Duarte, D. Baron, S. Sarvotham, K. F. Kelly, and R. G. Baraniuk, “A new compressive imaging camera architecture using optical-domain compression,” in *Computational Imaging IV*, vol. 6065. International Society for Optics and Photonics, 2006, p. 606509.
- [47] V. Antun, “Coherence estimates between Hadamard matrices and Daubechies wavelets,” Master’s thesis, 2016.
- [48] A. Hansen and L. Terhaar, “Sampling from binary measurements-on reconstructions from Walsh coefficients,” in *International Conference on Sampling Theory and Applications (SampTA)*. IEEE, 2017, pp. 256–260.

- [49] R. Calderbank, A. Hansen, B. Roman, and L. Thesing, “On reconstructions from measurements with binary functions,” *Springer, to appear*.
- [50] B. Fino, “Relations between Haar and Walsh/Hadamard transforms,” *Proceedings of the IEEE*, vol. 60, no. 5, pp. 647–648, 1972.
- [51] B. Falkowski and S. Rahardja, “Walsh-like functions and their relations,” *IEE Proceedings-Vision, Image and Signal Processing*, vol. 143, no. 5, pp. 279–284, 1996.
- [52] A. Thompson and R. Calderbank, “Compressive imaging using fast transform coding,” in *Emerging Imaging and Sensing Technologies*, vol. 9992. International Society for Optics and Photonics, 2016, p. 99920F.
- [53] H. M. Rafiq and M. U. Siddiqi, “The Haar-recursive transform and its consequence to the Walsh-Paley spectrum and the autocorrelation function,” *International Journal of Engineering Research and Application*, vol. 6, no. 11, pp. 46–58, 2016.
- [54] A. Hansen and L. Thesing, “On the stable sampling rate for binary measurements and wavelet reconstruction,” *Applied and Computational Harmonic Analysis*, 2018.
- [55] L. Thesing and A. C. Hansen, “Linear reconstructions and the analysis of the stable sampling rate,” vol. 17, pp. 103–126, 2018.
- [56] L. Thesing and A. Hansen, “Non uniform recovery guarantees for binary measurements and wavelet reconstructions,” *to appear*.
- [57] T. Blumensath and M. E. Davies, “Iterative hard thresholding for compressed sensing,” *Applied and computational harmonic analysis*, vol. 27, no. 3, pp. 265–274, 2009.
- [58] T. Zhang, “Sparse recovery with orthogonal matching pursuit under RIP,” *IEEE transactions on information theory*, vol. 57, no. 9, pp. 6215–6221, Sep. 2011.
- [59] T. T. Cai and A. Zhang, “Sparse representation of a polytope and recovery of sparse signals and low-rank matrices.” *IEEE transactions on information theory*, vol. 60, no. 1, pp. 122–132, 2014.
- [60] S. Mallat, *A wavelet tour of signal processing: the sparse way*. Academic press, 2008.
- [61] E. J. Stollnitz, A. DeRose, and D. H. Salesin, “Wavelets for computer graphics: a primer. 1,” *IEEE computer graphics and applications*, vol. 15, no. 3, pp. 76–84, 1995.
- [62] G. Beylkin, R. Coifman, and V. Rokhlin, “Fast wavelet transforms and numerical algorithms I,” *Communications on pure and applied mathematics*, vol. 44, no. 2, pp. 141–183, 1991.
- [63] R. D. Nowak and R. G. Baraniuk, “Wavelet-based transformations for nonlinear signal processing,” *IEEE transactions on signal processing*, vol. 47, no. 7, pp. 1852–1865, 1999.
- [64] R. A. DeVore, B. Jawerth, and B. J. Lucier, “Image compression through wavelet transform coding,” *IEEE transactions on information theory*, vol. 38, no. 2, pp. 719–746, 1992.

- [65] M. H. Neumann, R. Von Sachs *et al.*, “Wavelet thresholding in anisotropic function classes and application to adaptive estimation of evolutionary spectra,” *The Annals of Statistics*, vol. 25, no. 1, pp. 38–76, 1997.
- [66] J. Hadamard, “Resolution d’une question relative aux determinants,” *Bulletin des Sciences Mathématiques*, vol. 2, pp. 240–246, 1893.
- [67] S. Popa, “Classification of subfactors: the reduction to commuting squares,” *Inventiones mathematicae*, vol. 101, no. 1, pp. 19–43, 1990.
- [68] M. N. Kolounzakis and M. Matolcsi, “Complex Hadamard matrices and the spectral set conjecture,” *Collectanea mathematica*, vol. 57, no. 1, pp. 281–291, 2006.
- [69] J. J. Sylvester, “Thoughts on inverse orthogonal matrices, simultaneous signsuccessions, and tessellated pavements in two or more colours, with applications to newton’s rule, ornamental tile-work, and the theory of numbers,” *The London, Edinburgh, and Dublin Philosophical Magazine and Journal of Science*, vol. 34, no. 232, pp. 461–475, 1867.
- [70] L. Zhihua and Z. Qishan, “Ordering of Walsh functions,” *IEEE transactions on electromagnetic compatibility*, no. 2, pp. 115–119, 1983.
- [71] K. J. Horadam, *Hadamard matrices and their applications*. Princeton university press, 2012.
- [72] E. J. Candès, J. Romberg, and T. Tao, “Robust uncertainty principles: Exact signal reconstruction from highly incomplete frequency information,” *IEEE transactions on information theory*, vol. 52, no. 2, pp. 489–509, 2006.
- [73] E. Vandenberg and M. P. Friedlander, “Probing the pareto frontier for basis pursuit solutions,” *SIAM Journal on Scientific Computing*, vol. 31, no. 2, pp. 890–912, 2008.
- [74] —, “SPGL1: A solver for large-scale sparse reconstruction,” June 2007, <http://www.cs.ubc.ca/labs/scl/spgl1>.
- [75] “Spot - A Linear-Operator Toolbox,” retrieved on Aug. 25th, 2018. [Online]. Available: <http://www.cs.ubc.ca/labs/scl/spot/index.html>
- [76] D. L. Donoho and I. M. Johnstone, “Ideal spatial adaptation by wavelet shrinkage,” *Biometrika*, pp. 425–455, 1994.
- [77] L. A. Shepp and B. F. Logan, “The Fourier reconstruction of a head section,” *IEEE transactions on nuclear science*, vol. 21, no. 3, pp. 21–43, June 1974.
- [78] J. Granata, M. Conner, and R. Tolimieri, “Recursive fast algorithm and the role of the tensor product,” *IEEE transactions on signal processing*, vol. 40, no. 12, pp. 2921–2930, 1992.
- [79] C. F. Loan, “The ubiquitous Kronecker product,” *Journal of Computational and Applied Mathematics*, vol. 123, no. 1, pp. 85 – 100, 2000.
- [80] P. A. Regalia and M. K. Sanjit, “Kronecker products, unitary matrices and signal processing applications,” *SIAM review*, vol. 31, no. 4, pp. 586–613, 1989.

- [81] A. Fijany and C. P. Williams, “Quantum wavelet transforms: Fast algorithms and complete circuits,” in *NASA International Conference on Quantum Computing and Quantum Communications*. Springer, 1998, pp. 10–33.